

**T.R.
DICLE UNIVERSITY
INSTITUTE OF NATURAL AND APPLIED SCIENCES**

**CRYSTAL AND MOLECULAR STRUCTURE ANALYSIS OF
Dichloro[1,3-bis-(2-ethoxybenzyl)benzimidazole-2-ylidene] pyridine
palladium(II) AND Dichloro -[1-(2,3,4,5,6-pentametilbenzil)-3-
(2,3,5,6tetrametil) benzimidazol-2-yliden]Ruthenium (II)
BY SINGLE CRYSTAL X-RAY DIFFRACTION TECHNIQUE**

Sirwan Salih HASAN

MASTER THESIS OF SCIENCE

PHYSICS DEPARTMENT

**DİYARBAKIR
JUNE - 2015**

**T.C.
DICLE UNIVERSITY
INSTITUTE OF NATURAL AND APPLIED SCIENCES**

**CRYSTAL AND MOLECULAR STRUCTURE ANALYSIS OF
Dichloro[1,3-bis-(2-ethoxybenzyl)benzimidazole-2-ylidene] pyridine
palladium(II) AND Dichloro -[1-(2,3,4,5,6-pentametilbenzil)-3-
(2,3,5,6tetrametil) benzimidazol-2-yliden]Ruthenium (II)
BY SINGLE CRYSTAL X-RAY DIFFRACTION TECHNIQUE**

Sirwan Salih HASAN

MASTER THESIS OF SCIENCE

PHYSICS DEPARTMENT

SUPERVISED BY

Assoc. Prof. Dr. Ömer ÇELİK

**DİYARBAKIR
JUNE - 2015**

ACKNOWLEDGMENTS

I would like to acknowledge several people who supported me during my time as a Msc student.

Firstly, I would like to thank my supervisor Assoc. Prof. Dr. Ömer ÇELİK for his support, fruitful discussions, and meaningful input during all the time. I would also like to thank Assoc. Prof. Dr. Yusuf SELİM OCAK for filling the role of the secondary reviewer.

I would also like to thank to Firat ANĞAY, for being there and support me in several ways.

Finally, I would like to thank my family and friends for their support during the time of my thesis.

Sirwan Salih HASAN

MAY 2015

CONTEXT

ACKNOWLEDGMENTS	I
CONTEXT	II
ÖZET.....	IV
ABSTRACT	V
LIST OF TABLES	VI
LIST OF FIGURES	VII
LIST OF SYMBOLS	IX
1. INTRODUCTION.....	1
2. LITERATURE SUMMARY	3
3. MATERIAL AND METHOD.....	7
3.1. Synthesis	7
3.1.1. Synthesis of Single Crystal of Dichloro-[1,3-bis-(2- etoksibenzil)benzimidazole-2-yliden] pyridine palladium (II).....	7
3.1.2. Synthesis of Single Crystal of Dichloro -[1-(2,3,4,5,6-pentametilbenzil)-3- (2,3,5,6 tetramethyl) benzimidazole-2-yliden]Ruthenium (II).....	8
3.2. X-ray Crystallography.....	8
3.2.1. Basic Principles of X-ray Crystallography.....	8
3.2.2. Crystallinity	10
3.2.3. Historical Background of X-rays and Crystallography.....	10
3.2.4. Diffraction of X-ray by crystals	12
3.2.5. Crystal Structure and Symmetry	14
3.2.6. Point Group	18
3.2.7. Space Groups.....	18
3.2.8. Bragg's Law.....	20
3.2.9. Miller Indices.....	22
3.2.10. The Reciprocal Lattice and Ewald Sphere	22
3.2.11. The structure factor	24
3.3. X-rays and X-ray Generator.....	27

3.3.1 X-rays.....	27
3.3.2. Generation of X-rays.....	28
3.3.3. Synchrotron source X-ray generation	31
3.3.4. X-ray Detectors	31
3.3.5. The goniometer	33
3.3.5.1. Goniometer head	34
3.4. Single Crystal X-ray Diffraction.....	35
3.4.1. Introduction.....	35
3.4.2. Experimental Set-up.....	36
3.4.3. Data Collection Strategy	37
3.4.4. Device Information	38
3.4.5. Structure Solution.....	39
3.4.5.1. Stage 1 – Measurement of X-ray intensities.....	40
3.4.5.2. Stage 2 – The crystallographic phase problem and possible solutions....	42
3.4.5.2.1 Patterson Methods	43
3.4.5.2.2 Direct Methods	44
3.4.5.3 Stage 3 - Structure Refinement	44
4. FINDING AND DISCUSSION	47
4.1. Overview	47
4.2. Compound I: Dichloro[1,3-bis-(2-ethoxybenzyl)benzimidazole-2-ylidene] pyridine palladium(II)	47
4.3. Compound II: Dichloro-[1-(2,3,4,5,6-pentametilbenzil)-3-(2,3,5,6 tetramethyl) benzimidazole-2-ylidene] Ruthenium(II).....	62
5. RESULTS AND SUGGESTION	83
REFERENCES.....	85

ÖZET

X-IŞINLARI KIRINIM METODU İLE Dichloro[1,3-bis-(2-ethoxybenzyl)benzimidazole-2-ylidene] pyridine palladium(II) AND Dichloro-[1-(2,3,4,5,6-pentametilbenzil)-3-(2,3,5,6tetrametil) benzimidazol-2-yliden]Ruthenium (II) KOMPLEKSLERİNİN KRISTAL VE MOLEKULER YAPI ANALIZİ

YUKSEK LISANS TEZİ

Sirwan Salih HASAN

DİCLE ÜNİVERSİTESİ

FEN BİLİMLERİ ENSTİTÜSÜ

FİZİK ANABİLİM DALI

2015

Bu tez kapsamında yapılan temel çalışma, X-Işınlarını kristalografi çalışmasıdır. İçerik olarak, kimyasal formülleri arasında sıralanmış, Dichloro[1,3-bis-(2-ethoxybenzyl)benzimidazole-2-ylidene] pyridine palladium(II) ve Dichloro-[1-(2,3,4,5,6-pentametilbenzil)-3-(2,3,5,6 tetramethyl) benzimidazole-2-yliden]Ruthenium (II) metal kompleksinin molekül ve kristal yapılarına aydınlatılmaktadır.

- I. $ZnCl_2(C_8H_6N_2)_2$
- II. $ZnBr_2(C_8H_6N_2)_2$

Bilimsel ve endüstriyel alanda oldukça önemli olan bu komplekslerin yapılarına, WINGX paket programına kapsamında yer alan SHELXS97, SHELXL97, PARST97, PLATON2000 programlara ve CHEMDRAW ile ORTEPIII çizim programlara kullanılarak analiz edilmiştir. Gerekli deneysel veriler, Dicle Üniversitesi Bilim ve Teknoloji Araştırma ve Uygulama Merkezi X-Işınları laboratuvarında bulunan Bruker Breeze ApexII tipi kirinimetre ile elde edilmiştir.

Anahtar Kelimeler : Tek kristal X-Işınları kirinimi, Pd bileşiği, Ru bileşiği, WinGX.

ABSTRACT

CRYSTAL AND MOLECULAR STRUCTURE ANALYSIS OF Dichloro[1,3-bis-(2-ethoxybenzyl)benzimidazole-2-ylidene] pyridine palladium(II) AND Dichloro-[1-(2,3,4,5,6-pentamethylbenzyl)-3-(2,3,5,6-tetramethyl) benzimidazol-2-ylidene] Ruthenium (II) BY SINGLE CRYSTAL X-RAY DIFFRACTION TECHNIQUE

MASTER DEGREE THESIS

Sirwan Salih HASAN

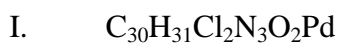
DICLE UNIVERSITY

INSTITUTE OF NATURAL AND APPLIED SCIENCES

PHYSICS DEPARTMENT

2015

The fundamental study reported in this thesis is X-ray crystallography work. In the scope, crystal and molecular structures of two compounds Dichloro[1,3-bis-(2-ethoxybenzyl)benzimidazole-2-ylidene] pyridine palladium(II) and Dichloro-[1-(2,3,4,5,6-pentamethylbenzyl)-3-(2,3,5,6 tetramethyl) benzimidazole-2-ylidene] Ruthenium(II). (Which their chemical formula have been given as follows) were revealed.



The structures of these complexes (having big importance in scientific and industrial area) were analyzed by using SHELXS97, SHELXL97, PARST97, PLATON2000 programmes located in WinGX package program and CHEMDRAW with ORTEP molecular drawing programs. Required experimental data were collected by Bruker Breeze ApexII CCD type diffractometer in X-ray laboratory of Dicle University, Science and Technological Research and Application Center.

Key Words: Single crystal X-ray diffraction, Pd complex, Ru complex, WinGX.

LIST OF TABLES

Table 3.1. The essential crystal symmetry and unit cell restrictions of the seven crystal systems.	16
Table 4.1. Sumamry of crystallographic data for compound (I)	49
Table 4.2. Atomic bond lengths (Å) of compound (I).....	52
Table 4.3. Atomic bond lengths (Å) of compound (I).....	53
Table 4.4. Analysis of Short Ring-Interactions	54
Table 4.5. Hydrogen-bond geometry (Å, °) of compound (I)	55
Table 4.6. Fractional atomic coordinates and isotropic or equivalent isotropic displacement parameters (Å ²) of compound (I).....	60
Table 4.7. Atomic displacement parameters (Å ²) of compound compound (I)	61
Table 4.8. Sumamry of crystallographic data for compound (II).....	63
Table 4.9. The comparison of the peak differences in electron desnity map of previous studies.....	65
Table 4.10. Dihedral angles formed by LSQ-planes.....	66
Table 4.11. Analysis of Short Ring-Interactions	66
Table 4.12. Hydrogen-bond geometry (Å, °) of compound (II).....	67
Table 4.13. Fractional atomic coordinates and isotropic or equivalent isotropic displacement parameters (Å ²) of compound (II).....	72
Table 4.14. Atomic displacement parameters (Å ²) of compound (II)	75
Table 4.15. Atomic bond lengths (Å) of compound (II)	77
Table 4.16. Atomic bond angles (deg) of compound (II).....	79

LIST OF FIGURES

Figure 3.1. Chemical scheme of $C_{30}H_{31}Cl_2N_3O_2Pd$	7
Figure 3.2. Chemical scheme of $C_{37}H_{54}C_{12}N_2Ru$	8
Figure 3.3. A single crystal	10
Figure 3.4. An example of a diffraction pattern. The particular position and symmetry of the spots is illustrated in addition to the varying intensities of the spots.	13
Figure 3.5. Demonstration of the crystal lattice, created by representing the constituent units with points	14
Figure 3.6. An example of a unit cell with the axes and angles labelled.	15
Figure 3.7. The fourteen Bravais lattices with the lattice points displayed.	17
Figure 3.8. The effect a 2_1 screw axis has upon a particular point.....	19
Figure 3.9. An X-ray beam makes angle θ with a set of planes with inter planar spacing d . For constructive interference $n \lambda = 2d \sin \theta$	21
Figure 3.10. A pictorial representation of the 111 Miller plane.....	22
Figure 3.11. A pictorial representation of the 010 Miller plane.....	22
Figure 3.12. Diffraction in belongs to the reciprocal lattice.	23
Figure 3.13. Axial components of the point x,y,z	25
Figure 3.14. Schematic diagram for application of X-rays in modern science and technology	27
Figure 3.15. Emission of $K\alpha$ and $K\beta$	28
Figure 3.16. A schematic diagram of an X-ray tube (L.J. Poppe et al., 2001).....	29

Figure 3.17. SMART APEXII goniometer elements-adapted from (Bruker advanced X-ray solutions- APEXII user manual version 1.22)	34
Figure 3.18. Schematic illustrating set-up for a single crystal X-ray diffraction experiment.....	37
Figure 3.19. some components of SMART APEX system.....	39
Figure 3.20. A crystal mounted on the tip using epoxy. Pictures via a high magnification video camera present on the diffractometer.....	41
Figure 4.1. Molecular structure of Compound (I) (Dichloro-[1,3-bis-(2-etoksibenzil)benzimidazole-2-yliden] pyridine palladium (II)) (ORTEP diagram)	50
Figure 4.2. Geometric Coordinate of the palladium atom	51
Figure 4.3. Intramolecular hydrogen bonds (dashed lines) of compound (I).....	56
Figure 4.4. Unit Cell packing of compound (I) at (100)	57
Figure 4.5. Unit Cell packing of compound (I) at (010)	58
Figure 4.6. Unit Cell packing of compound (I) at (001)	59
Figure 4.7. Molecular structure of of Dichloro-[1,3-bis-(2-etoksibenzil)benzimidazole-2-yliden] pyridine palladium (II) (ORTEP diagram).....	64
Figure 4.8. Geometric Coordinate of the ruthenium atom	65
Figure 4.9. Intramolecular hydrogen bonds (dashed lines) compound (II).....	68
Figure 4.10. Unit Cell packing of compound (II) at (100).....	69
Figure 4.11. Unit Cell packing of compound (II) at (010).....	70
Figure 4.12. Unit Cell packing of compound (II) at (001).....	71

LIST OF SYMBOLS

Symbols	Definition
α	Alpha
β	Beta
γ	Gamma
Å	Ångstrom
I	Body centred
C	C centred
°	Degrees
F	Face centred
K	Kelvin
3D	Three dimensional
XRD	X-ray Diffraction
CCD	Charge-Coupled Device
CCDC	Cambridge Crystallographic Data Center
CIF	Crystallographic Information File
Goof	Goodness of Fit
IP	Image Plate area detector
ORTEP	Oak Ridge Thermal Ellipsoids Plot
R_{int}	Internal Reliability Index
RCM	Ring-Closing Metathesis reaction
SADABS	Siemens Area Detector Absorption Correction

SAINT	SAX Area-detector Integration (SAX-Siemens Analytical X-ray)
SMART	Siemens Molecular Analysis Research Tool
wR	weighted Reliability Index
<i>hkl</i>	Miller Indices (<i>hkl</i>)
mm	Millimetre
Mol	Moles
Nm	Nanometre
<i>h</i>	Planck Constant
P	Primitive
R_1	<i>R</i> -factor
σ	Sigma
f_j	Structure factor
i.e.	That is
θ	Theta
V	Volume
λ	Wavelength
wR2	Weighted <i>R</i> -factor
XAS	X-ray absorption spectroscopy

1. INTRODUCTION

The technology of X-ray has developed into one of the most notable methods of structural analysis during the past century, as evidenced by how its discovery and enhancements play an important role in daily living. Versatility is an attribute of X-ray technology, offering widespread use in many areas. It is beneficial not only to the scientist, but also to health professionals and law enforcement officers. More importantly, the chemical structure determination of various molecules is indispensable to both physicists and chemists in an effort to gain insight into chemical problems. A few physical methods are utilized to determine material structures, and amongst these methods, X-ray diffraction techniques have been the most successful.

When the German physicist Wilhelm Röntgen discovered the X-ray in 1895, was speedily followed by the demonstration by von Laue of diffraction of X-rays by crystals (Friedrich et al., 1952). With the addition of W.L. Bragg's diffraction theory in 1912, this non-destructive analytical technique has become extremely successful since it is one of few "fingerprinting" methods that can be used to accurately characterize both the identity and amount of compounds found in any crystalline system.

It is known that any material which is consisted of an ordered array of atoms will give a diffraction pattern. The three-dimensional structure determinations of compounds are most easily achieved by single-crystal X-ray diffraction. Single-crystal X-ray diffraction analysis method differs from other diffraction methods because the measurement of the diffraction pattern in this method is produced when the single crystal sample is oriented. The scattering of x-rays at long range ordered periodic systems is in general called x-ray diffraction. These systems are typically crystals. The scattering at these periodic structures cause constructive and destructive interference of the scattered waves resulting in spots of very high intensity. These spots are called Bragg peaks or Bragg reflections. The diffraction pattern produced depends on the current atoms, their locations, and thermal motion. Newer experiments use an X-ray detector based on the charge coupled device (CCD) camera technology, and the diffraction pattern from a single crystal yields a three dimension intensity distribution that appears as a series of "spots" in the detector image. From Fourier series analysis

and least-squares refinement of the intensities of the spots allows us accurate determination of the chemical identity and molecular structure of the sample.

In principle an X-ray diffraction analysis can be performed in any kind of material. Nevertheless in most of the cases the materials are solid samples. Only in some quite specific applications the samples are liquid and in very special cases gases. Furthermore in single crystal X-ray diffraction, as an additional distinction, the size of the single crystal should be small, preferably in the range about 0.1 to 0.2 mm (Klug et al., 1974). X-ray crystallography is therefore the only one capable of providing detailed information on interatomic distances, bond angles, molecular architecture, absolute configuration, thermal vibration parameters, crystal packing, as well as possible order-disorder and/or non-stoichiometry from the same experiment (Lee et al., 1994)

The X-ray structural analysis we will be provided with the information of the bond lengths, bond angles, conformation, coordination and other crystallographic information and details of the molecular structure of the Dichloro-[1,3-bis-(2-etoksibenzil)benzimidazole-2-yliden]pyridine palladium (II) and Dichloro-[1-(2,3,4,5,6-pentametilbenzil)-3-(2,3,5,6 tetramethyl) benzimidazole-2-yliden]Ruthenium (II)

The determination of a crystal structure normally proceeds in three stages. The first is the measurement of the intensities of the Bragg reflections and the calculation from them of amplitudes (observed structure factors), reduced to a common scale and corrected for various geometrical and physical factors, and observed structure amplitudes calculated. The second stage is solving the phase problem of X-ray diffraction, the problem that only the intensities of the diffraction pattern are recorded, whereas the phases of the reflections cannot be measured directly (the phase information is lost). We must therefore find a way to assign initial, approximation phases (solve the structure). For small molecules, for example, the structures can be solved in this thesis by so-called 'direct methods' using the SHELX-97 program. The third stage involves refining the approximate atomic positions in order to obtain the best possible agreement between the observed structure factors and the calculated structure factors.

2. LITERATURE SUMMARY

Crystallography is the most unambiguous method for determining structure of small molecules and macromolecules, and single crystal X-ray diffraction provides accurate and precise measurements of molecular dimensions.

The study reported in this thesis is an X-ray crystallography work. The most effective method to analyse crystal structure is the single-crystal X-ray diffraction method. According to this principle, the molecular and crystal structure of Dichloro[1,3-bis-(2-ethoxybenzyl)benzimidazole-2-ylidene] pyridine palladium(II), and Dichloro -[1-(2,3,4,5,6-pentametilbenzil)-3-(2,3,5,6tetrametil) benzimidazol-2-ylidene]Ruthenium(II) are reported in this study the synthesis. In structure refinements and solutions; the intensity data collected on the Bruker Smart ApexII diffractometer.

The molecular and crystal structure of samples are refined and solved by WinGX package program.

The first small molecule was crystallised in the tetragonal space group $P4_12_12$. The second small molecule was crystallised in the monoclinic space group $P2_1/n$. The structure was solved with an R factor of 0.0697. In addition the crystal packing of two small molecules was analysed. The implications of the determined crystal structures are discussed in terms of the relevant literature in each case.

The results of X-ray structure analyses of two such complexes, namely, Bis(acetato-O)bis(pyridine-N)palladium(II) Monohydrate and Bis(acetato-O)bis-(diethylamine-N)palladium(II) was reported by SVETLANA V. et al., (1996) they found in both title complexes, the Pd atom has square planar coordination. Also they found the Pd-N bond is longer in Bis(acetato-O)bis-(diethylamine-N)palladium(II) 2.066(2) Å than in Bis(acetato-O)bis(pyridine-N)palladium(II) 2.010(4) Å.

Cheng et al., (2002) reported Dichloro[2,2'-hydroxy(ethoxy)methylene-dipyridine- k^2N,N']palladium(II). They found that in this complex the central Pd(II) atom is bonded to two pyridine N atoms and two terminal Cl atoms and the coordination geometry of the Pd atom is square planar with a slight tetrahedral distortion. The two

Pd-N distances calculated as 2.029(3) and 2.057(3) Å, and the N-Pd-N angle is 86.56(13)°. Also, the two Pd-Cl distances calculated as 2.2929(11) and 2.2959(11) Å, and the Cl-Pd-Cl angle is 90.84(5)°.

Also Hsueh et al., (2006) reported Dichloro{(E)-2,4,6-trimethyl-N-[1-(2-pyridyl)-ethylidene]aniline-*k*²N,N'}palladium(II) acetonitrile solvate. They solve molecular and crystal structure of this compound and found that the Pd atom has square planar coordination by two N and two Cl atoms and crystal packing is stabilized by C-H...Cl interactions. The two Pd-N distances calculated as 2.022(3) and 2.028(3) Å, and the N-Pd-N angle is 79.92(13)°. Also, the two Pd-Cl distances calculated as 2.2780(11) and 2.2916(11) Å, and the Cl-Pd-Cl angle is 90.37(5)°.

Ojwach et al. (2008) are reported synthesis, molecular structures, and activation of small molecules of (Pyrazol-1-ylmethyl)pyridine palladium complexes. They solve molecular and crystal structure of (Pyrazol-1-ylmethyl) pyridine palladium complexes. Pd-N and Pd-Cl bonds are calculated as 2.048(3) Å and 2.2802(10) Å' respectively.

Preparation of the Pd(II) complexes containing 2-(4-R-1,2,3-triazol-1-yl)pyridine [R=C₆H₅ (1), NC₅H₄(2)] was described by Jindabot et al., (2013) in the report name Palladium(II) complexes featuring bidentate pyridine-triazole ligands: Synthesis, structures, and catalytic activities for Suzuki-Miyaura coupling reactions. They found both complexes crystallized in the P21/c space group. All non-hydrogen atoms were refined anisotropically while the hydrogen atoms were placed in calculated positions and not refined. However they found Crystal structures of 1 and 2 revealed a square planar geometry, Pd-N1, Pd-N2, Pd-Cl1 and Pd-Cl2 calculated as 2.054(5) Å, 2.014(5) Å, 2.271(2) Å and 2.274(2) Å' respectively for complex (1) and 2.066(2) Å, 1.999(2) Å, 2.270(1) Å and 2.275(1) Å' respectively for complex (2).

Çetinkaya et al., (1998) determined the crystal structure of complex Ru(II) by the X-ray diffraction in the report Ruthenium(II) complexes with 2,6-pyridyl-diimine ligands: synthesis, characterization and catalytic activity in epoxidation reactions. They found the Pd(II) atom has octahedral coordination.

Huxham et al., (2003) reported the synthesis, structural characterization, and in vitro anti-cancer activity of chloro(*p*-cymene) complexes of ruthenium(II) containing a disulfoxide ligand. The crystal structure of two complex R(II) $[\text{RuCl}_2(\textit{p}\text{-cymene})]_2(\textit{m}\text{-BESE})$ and $[\text{RuCl}(\textit{p}\text{-cymene})(\textit{BESE})]\text{PF}_6$ was determined by X-ray crystallography. The structure of two complexes was solved by direct methods and expanded used Fourier techniques; the H atoms was included at calculated positions, but not refined. They found the central Ru(II) atom is bonded to six C atoms, two Cl atoms and one S atom, the coordination geometry of the Ru(II) atom is square planar Pseudo tetrahedral coordinate.

Imhof et al., (2005) reported Tetrakis(tert-butyl isocyanide-2*k*C)dichloro-1*k*Cl,3*k*Cl-di- μ -cyano-1*k*N:2*k*C;2*k*C:3*k*N-bis[1,3(*n*⁴)-cycloocta-1,5-diene]dirhodium(I)-ruthenium(II) They solve molecular and crystal structure of $[\text{Rh}_2\text{Ru}(\text{CN})_2\text{Cl}_2(\text{C}_8\text{H}_{12})_2(\text{C}_5\text{H}_9\text{N})_4]$. They found the molecular structure of the Ru atom in a nearly ideal octahedral coordination geometry, whereas the Rh atoms are situated in square-planar ligand environments. The central ruthenium ion was located on a crystallographic twofold axis.

Chiririwa et al., (2011) reported Bis(acetonitrile-*j*N)dichlorido(*g*4-cycloocta-1,5-diene)ruthenium(II) acetonitrile monosolvate. They solve molecular and crystal structure of $[\text{RuCl}_2(\text{C}_8\text{H}_{12})(\text{C}_2\text{H}_3\text{N})_2] \cdot \text{CH}_3\text{CN}$, they found the coordination about the Ru(II) atom can thus be considered to be octahedral with a slightly trigonal distortion.

Lu et al., (2009) reported Synthesis, structure and catalytic activities for the hydrogen transfer reactions of the ruthenium(II) carbonyl chloride complexes with pyridine-2,6-diimine. They solve molecular and crystal structure of two Ru(II) carbonyl chloride complexes with pyridine-2,6-diimine, (L)Ru(CO)Cl₂ (L=2,6-diacetylpyridinebis(2,4,6-trimethylanil), **1**; L=2,6-diacetylpyridinebis(2,6-diisopropylanil), **2**). The structure of two compound was determined by X-ray crystallography, which show the distorted octahedral geometry around Ru(II).

Brietzke et al., (2014) reported Crystal structure of (2,11-diaza[3.3](2,6)pyridinophane-*k*⁴N,N',N'',N''')(1,6,7,12-tetraazaperylen-*k*²N¹,N¹²) ruthenium(II) bis(hexafluoridophosphate) acetonitrile 1.422-solvate . they solve crystal

structure of compound compound, $[\text{Ru}(\text{C}_{14}\text{H}_{16}\text{N}_4)(\text{C}_{16}\text{H}_8\text{N}_4)](\text{PF}_6)_2 \cdot 1.422\text{CH}_3\text{CN}$ was used X-ray diffraction technology to this work, they found the Ru(II) atom was coordinated in a distorted octahedral geometry, particularly manifested by the $\text{N}_{\text{amine}}\text{-Ru-N}_{\text{amine}}$ angle of $153.79(10)^\circ$.

Ma et al., (2015) reported Ruthenium sensitizers with various 2-thiophenimidazo[4,5-f][1,10] phenanthroline based ancillary ligands and their performance for dye-sensitized solar cells. They solved molecular and crystal structure of three compounds $\text{C}_{27}\text{H}_{24}\text{C}_{12}\text{N}_4\text{RuS}$, $\text{C}_{29}\text{H}_{31}\text{BrC}_{12}\text{N}_4\text{O}_2\text{RuS}$ and $\text{C}_{28}\text{H}_{31}\text{BrC}_{12}\text{N}_4\text{O}_3\text{RuS}$, in each compounds found that the Ru(II) centre bonded to six C atoms, two N atoms and one Cl atom shows a pseudo-tetrahedral coordinate.

3. MATERIAL AND METHOD

3.1. Synthesis

The synthesis of our crystal which we refined and solved their molecular and crystal structure were synthesised by Dr. Sedat Yasar, his work group at the University of Inonu, Malatya, Turkey.

3.1.1. Synthesis of Single Crystal of Dichloro-[1,3-bis-(2-*etoksibenzil*)benzimidazole-2-yliden] pyridine palladium (II)

The palladium-NHC complex was synthesized with method reported by Organ (O'Brien et al., 2006). In air, a pressure tube was charged with PdCl₂ (87 mg, 0.5 mmol), NHC.HCl (0.55 mmol), and K₂CO₃ (345 mg, 2.5 mmol). 3 mL of pyridine was added. The reaction mixture was heated with vigorous stirring for 10 h at 80 °C. The reaction mixture was then diluted with sufficiently dichloromethane (DCM) until the product was recovered. The DCM was evaporated, and the pyridine was vacuum-distilled. Residue solid was washed with hexane (2x10 mL) and diethyl ether (2x10 mL) and then dried in vacuo. Molecular structures of NHC–Pd–pyridine complexes were determined by NMR, LC-MS(ESI), IR and micro analyses. The chemical scheme of C₃₀H₃₁Cl₂N₃O₂Pd can be seen in Figure 3.1.

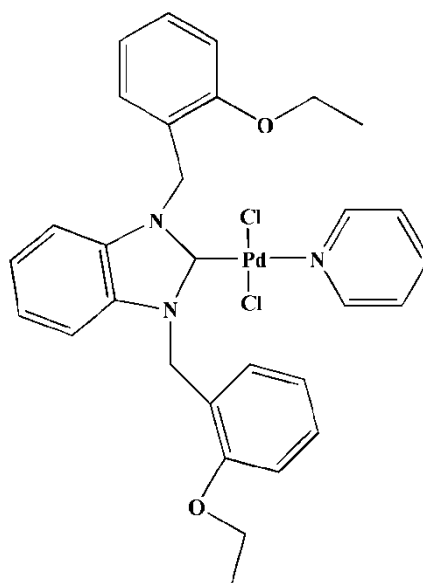


Figure 3.1. Chemical scheme of C₃₀H₃₁Cl₂N₃O₂Pd

3.1.2. Synthesis of Single Crystal of Dichloro -[1-(2,3,4,5,6-pentamethylbenzil)-3-(2,3,5,6 tetramethyl) benzimidazole-2-yliden]Ruthenium (II)

1 salt (2.9 mmol), Cs_2CO_3 (2.9 mmol), $[\text{RuCl}_2(p\text{-simen})]_2$ (1.45 mmol) and molecular were vacuuming in elek schlenk at 100 °C. After that 30 mL of dry toluen was added, the reaction mixture was heated at 90 °C and after that It was heated for 4 h at 120 °C. Toluene was disposed at vacuum. CH_2Cl_2 was added over it and filtered. After CH_2Cl_2 was added, claret red crystal was created. The chemical scheme of $\text{C}_{37}\text{H}_{54}\text{Cl}_2\text{N}_2\text{Ru}$ can be seen in Figure 3.2.

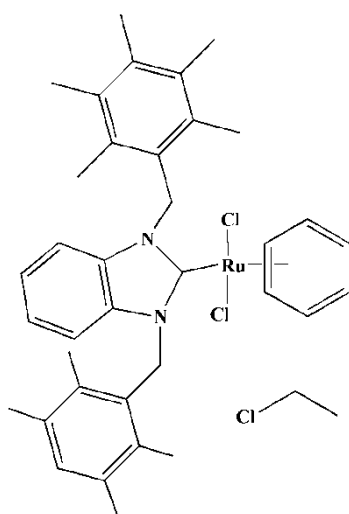


Figure 3.2. Chemical scheme of $\text{C}_{37}\text{H}_{54}\text{Cl}_2\text{N}_2\text{Ru}$

3.2. X-ray Crystallography

3.2.1. Basic Principles of X-ray Crystallography

Single-crystal X-ray diffraction, denoted to as X-ray crystallography, is a study of crystal structure by X-ray diffraction techniques. This causes to an understanding of the molecular and crystal structure of a substance. Because a single molecule does not have sufficient diffraction power, the regular arrangement of molecules in a crystal is a needful to reinforce scattering from one molecule by all others. Crystals are objects (molecules, atoms, and ions) coordinated in a regularly repeating pattern in three dimensions from smaller units, so-called 'unit cells'. It generates the complete crystal by 3D translation along the unit cell axis.

The basis of X-ray crystallography is the interaction of matter in the crystalline case with X-rays. Since the wave-lengths of X-rays (in the nanometer range) are of the same domain of magnitude as of the interatomic distances within the crystal, the interaction results in the X-ray diffraction. This method can be used to determine the molecule crystal structure at atomic resolution: the composition of atoms, their relative orientation, and the chemical bonds between the atoms (both bond lengths and bond angles).

A simple analogy to help visualise the basic principles that underpin X-ray crystallography is that of a simple optical microscope. In both microscopy and crystallography it is useful to view radiation in terms of a travelling wave of energy as opposed to a particle (Eric Lifshin, 1999).

In the case of the optical microscope a light source provides visible light waves which pass through the sample under study and are subsequently diffracted. Each of these diffracted waves has a characteristic intensity and phase associated with it. These intensities and phases are then recombined by a lens in order to form an image.

As the name suggests X-ray crystallography utilises X-rays as opposed to visible light. They are used as they are easily accessible and possess wavelengths comparable to bond lengths allowing for visualisation down to the atomic level.

However the use of X-rays poses a problem – there is no known method capable of recombining the scattered X-rays and thus forming an image. The intensity of the diffracted waves can easily be determined by using an X-ray sensitive detector or photographic plate. Unfortunately the phase information of the waves has been lost. This is the physical basis of the phase problem that is inherently present within crystallography (Shafranovskii et al., 1962)

Instead a branch of mathematics known as Fourier series are used in place of a lens to recombine the scattered X-rays.

Technically the terms “scattered” and “diffracted” describe different wave-obstacle phenomenon. Scattering is results in the wave changing direction with no form of interference produced

In comparison diffraction wavelength results in a change of direction of the wave as well as the production of constructive and destructive interference. Therefore technically it is diffraction and not scattering that produces the patterns observed in crystallography (Woolfson et al., 1997).

3.2.2. Crystallinity

Crystalline materials consist of regular arrays of atoms, ions or molecules in three dimensions, with interatomic distances of approximately 1\AA . In order for diffraction to occur, the wavelength of the incident light has to be of the same order of magnitude as the spacings of the diffraction grating (i.e. the crystal). Because of the periodic nature of their internal structures, crystals (figure 3.3) can act as a three dimensional diffraction grating to radiation of a suitable wavelength (X-rays), and the resulting diffraction pattern generated can be interpreted to give the internal positions of atoms within a crystal very accurately (L. Smart et al., 2001).



Figure 3.3. A single crystal

3.2.3. Historical Background of X-rays and Crystallography

X-ray technology has more than a hundred years of history and its discovery and development has revolutionized many areas of modern science and technology. X-rays were discovered by the German physicist Wilhelm Conrad Rontgen in 1895, who was honored with the Nobel Prize for Physics in 1901. In many languages today, X-rays are still referred to as Rontgen rays or Rontgen radiation. The mysterious light was found

that's invisible to human eyes, but capable of penetrating opaque objects and exposing photographic films (S. P. Timoshenko et al., 1970). The density contrast of the object is disclosed on the developed film as a radiograph. Since then, X-rays have been developed for medical imaging, for example, for detection of bony structures and diseases in soft tissues such as pneumonia and lung cancer. X-rays have also been used to treat diseases. Radiotherapy employs high-energy X-rays to generate a curative medical intervention to the cancer tissues. A modern technology, tomotherapy, combines the precision of a computerized tomography scan with the potency of radiation treatment to selectively destroy cancerous tumors while minimizing harm to surrounding tissue. Today, medical diagnoses and treatments are still the most common use of X-ray technology. The phenomenon of X-ray diffraction by crystals was discovered in 1912 by Max Von Laue. The diffraction condition in a simple mathematical form, which is now known as the Bragg law, was formulated by Lawrence Bragg in the same year. The Nobel Prizes for Physics in two consecutive years (1914 and 1915) were awarded to von Laue and the senior and junior Bragg for the discovery and explanation of X-ray diffraction. X-ray diffraction techniques are based on elastic scattered X-rays from matter. Due to the wave nature of X-rays, the scattered X-rays from a sample can interfere with each other such that the intensity distribution is determined by the wavelength and the incident angle of the X-rays and the atomic arrangement of the sample structure, particularly the long-range order of crystalline structures.

The expression of the space distribution of the scattered X-rays is referred to as an X-ray diffraction pattern. The atomic level structure of the material can then be determined by analyzing the diffraction pattern. Over its hundred-year history of development, X-ray diffraction techniques have developed into many specialized fields.

Each has its specialized instruments, samples of interests, theory, and practice. Single crystal X-ray diffraction (SCD) is a technique used to solve the complete structure of crystalline materials, typically in the form of single crystals. The technique started with simple inorganic solids and grew into complex macromolecules. Protein structures were first determined by X-ray diffraction analysis by Max Perutz and Sir John Cowdery Kendrew in 1958 and both shared the 1962 Nobel Prize in Chemistry.

Today, protein crystallography is the dominant application of SCD. X-ray powder diffraction (XRPD), alternatively powder X-ray diffraction (PXRD), got its name from the technique of collecting X-ray diffraction patterns from packed powder samples. Generally, X-ray powder diffraction involves the characterization of the crystallographic structure, crystallite size, and orientation distribution in polycrystalline samples.

X-ray diffraction (XRD), by definition, covers single-crystal diffraction and powder diffraction as well as many X-ray diffraction techniques. However, it has been accepted as convention that SCD is distinguished from XRD. By this practice, XRD is commonly used to represent various X-ray diffraction applications other than SCD. These applications include phase identification, texture analysis, stress measurement, percent crystallinity, particle (grain) size, and thin film analysis. An analogous method to X-ray diffraction is small-angle X-ray scattering (SAXS) technique. SAXS measures scattering intensity at scattering angles within a few degrees from the incident angle. SAXS pattern reveals the material structures, typically particle size and shape, in the nanometres to micrometres range. In contrast to SAXS, other X-ray diffraction techniques are also referred to as wide-angle X-ray scattering (WAXS) (BOB, 2009).

3.2.4. Diffraction of X-ray by crystals

In theory a single molecule could be irradiated in order to produce a diffraction pattern. However in practice this would lead to an immeasurably weak pattern and rapid degradation of the molecule by the X-rays. Crystals are highly ordered structures which are composed of a regular arrangement of units (these units could be atoms, molecules or ions) that is repeated infinitely in three dimensions. Therefore instead of having one unit in a particular orientation there are now in effect an infinite number – this leads to “reinforcement” of the diffraction pattern and hence an averaged data set. In addition due to the huge amount of identical units radiation damage is usually negligible.

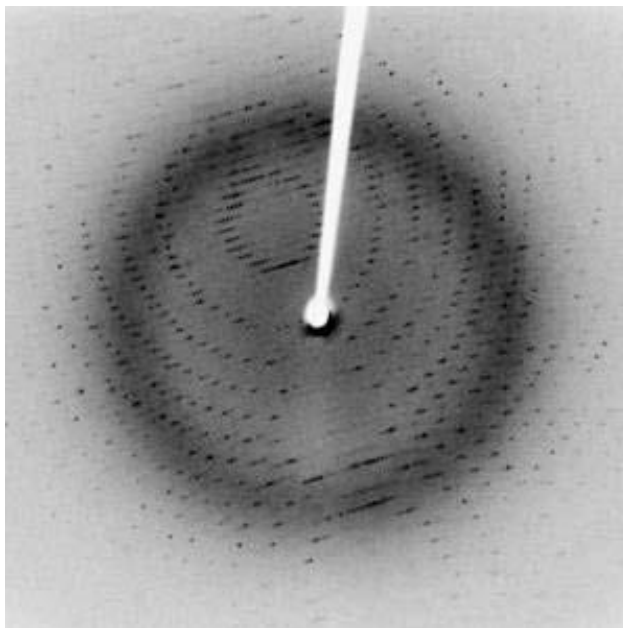


Figure 3.4. An example of a diffraction pattern. The particular position and symmetry of the spots is illustrated in addition to the varying intensities of the spots.

To create diffraction pattern a crystal is bathed in a beam of X-rays. The regular arrangement of the atoms present in the crystal acts as a three dimensional diffraction grating. The incident X-rays interact with the electrons of the crystal via inelastic collisions which causes diffraction. The result is a pattern consisting of spots which possesses three important properties directly related to the crystal under study Figure 3.4.

The position, symmetry and intensity of the spots all hold information that must be extracted.

However, one diffraction pattern is not sufficient to allow for structure determination. This is because that only a small number of reflections will be excited at the particular angle of the stationary crystal. As a result the crystal must be slowly rotated (through small increments) whilst still fully immersed within the X-ray beam. In modern day diffractometers this a a fully automated, computer controlled process which results in the maximum number of reflections being recorded.

The X-rays most commonly used in “home” laboratory based experiments are monochromated MoK α ($\lambda = 0.71\text{\AA}$) and CuK α ($\lambda = 1.54\text{\AA}$). These particular wavelengths are favoured as they are comparable with the distances under study. (E.g. C-C = 1.54\AA). This helps to ensure appreciable diffraction occurs.

3.2.5. Crystal Structure and Symmetry

As a consequence of their highly ordered structure, crystals also display a high degree of symmetry. This symmetry is described by a number of different concepts which are subsequently defined.

As previously mentioned crystals are composed of a regular, repeating arrangement of units. If each of the constituent units was represented by a single point then the resulting array would be representative of the repeating nature of the crystal. This array of points (related to each other by translational symmetry) is known as the lattice of the crystal Figure 3.5.

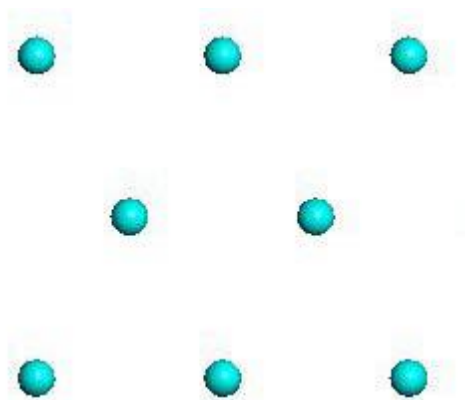


Figure 3.5. Demonstration of the crystal lattice, created by representing the constituent units with points

An extension upon the theme of lattice points is the unit cell. A unit cell is a parallelogram consisting of four lattice points. Crystals are defined by their unit cells they describe the simplest “building block” that is repeated in three dimensions to produce the bulk crystal (Cullity, 1956). Each unit cell is defined in terms of lattice points. The lattice is the basic network of points on which the repeating unit (the contents of the unit cell) may be imagined to be laid down so that the regularly repeating structure of the crystal is obtained. Thus the lattice establishes the repeating pattern (Moore, 2008).

A unit cell is characterised by three vectors a , b and c which lie along the x, y and z directions respectively. Also of importance are the angles between these vectors – α alpha, β beta and γ gamma. Convention dictates that alpha is the angle between vectors b and c , beta is the angle between vectors a and c whilst gamma is the angle between a and b (Figure 3.6).

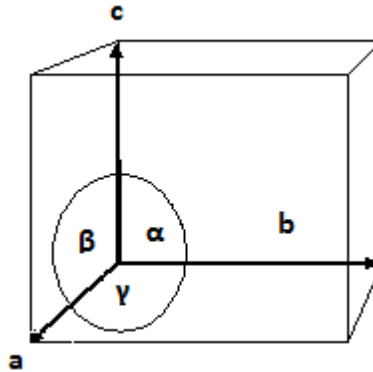


Figure 3.6. An example of a unit cell with the axes and angles labelled.

These vectors and the angles between them give rise to the seven crystal systems which are used to describe the geometry of the unit cell. Rotational and reflection symmetry place restrictions on the allowed vector lengths and angles. These restrictions allow for classification into seven groups – triclinic, monoclinic, orthorhombic, tetragonal, trigonal, hexagonal and cubic. The aforementioned restrictions are given in Table 3.1.

Table 3.1. The essential crystal symmetry and unit cell restrictions of the seven crystal systems.

Crystal system	Unit cell restrictions	Essential symmetry of crystal
<i>Triclinic</i>	None	None
<i>Monoclinic</i>	One diad axis (2 fold rotation) or mirror plane (inverse diad axis)	$a \neq b \neq c$ $\beta \neq \alpha = \gamma = 90^\circ$
<i>Orthorhombic</i>	Three orthogonal diad axes or inverse diad axes	$a \neq b \neq c$ $\alpha = \beta = \gamma = 90^\circ$
<i>Tetragonal</i>	One tetra axis (four fold rotation) or inverse tetrad axis	$a = b = c$ $\alpha = \beta = \gamma = 90^\circ$
<i>Trigonal</i>	One triad (three fold rotation) axis or inverse triad axis	$a = b = c$ $\alpha = \beta = \gamma \neq 90^\circ$
<i>Hexagonal</i>	One hexad (five fold rotation) axis or inverse hexad axis	$a = b \neq c$ $\alpha = \beta = 90^\circ, \gamma = 120^\circ$
<i>Cubic</i>	Four triad axes or inverse triad axes	$a = b = c$ $\alpha = \beta = \gamma = 90^\circ$

Introducing translational symmetry into the seven crystal systems (which only include rotational and reflection symmetry) forms the Bravais (or space) lattices. There are 14 possible Bravais lattices which involve four different ways of centring the lattice points Figure 3.7. The possible lattice centring are:

- Simple (Primitive) (P) – Lattice points are located at the corners of the unit cell.
- Body Centred (I) – All primitive points included plus an additional point at the centre of the unit cell.
- Base Centred (C) – All primitive points included plus an additional point at the centre of one face of the unit cell.
- Face Centred (F) – All primitive points included plus an additional points at the centre of each face of the unit cell.

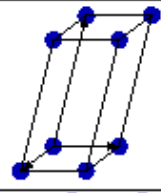
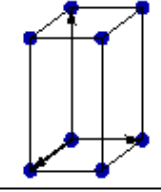
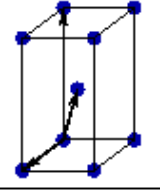
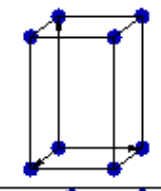
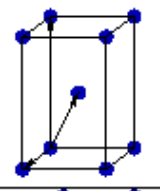
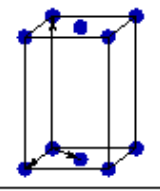
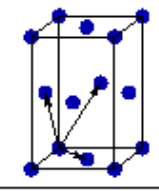
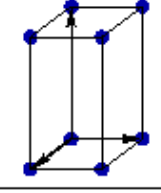
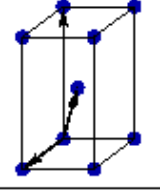
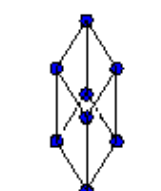
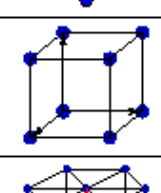
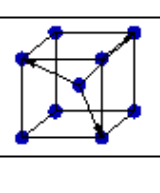
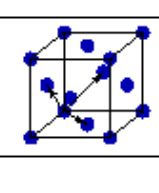
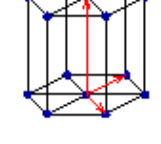
Bravais lattice	Simple (P)	Body Centred (I)	Base Centred (C)	Face Centred (F)
<i>Triclinic</i>				
<i>Monoclinic</i>				
<i>Orthorhombic</i>				
<i>Tetragonal</i>				
<i>Trigonal</i>				
<i>Cubic</i>				
<i>Hexagonal</i>				

Figure 3.7. The fourteen Bravais lattices with the lattice points displayed.

3.2.6. Point Group

A point group is a mathematical descriptor for a group of symmetry operations that pass through a central point. These symmetry operations must leave at least one point unchanged and the appearance of the object unaltered.

There are four symmetry operations associated with point groups

1. n -fold rotation axes: a rotation through $(360^\circ/n)$ which leaves the object unaltered (where n is an integer).
2. Mirror planes: involves a reflection which takes place with respect to a mirror plane.
3. Inversions: involves moving every point x, y, z to $-x, -y, -z$.
4. Improper rotations: a rotation followed by an inversion.

Compared to the point groups for an isolated object (such as a single molecule) there are 230 possible crystallographic space groups. This is because there are 32 possible ways to combine the point group symmetry operations with the translational symmetry inherently present within crystals (crystallographic restriction theorem) (Molloy, 2004).

3.2.7. Space Groups

The combination of non-translational and translational symmetry elements combined with the fourteen Bravais lattices, generate 230 unique combinations of packing three-dimensional space known as space groups. These space groups are unequally distributed across the seven crystal systems, and determination of a space group from crystal data is achieved by looking at absences within the data.

Space groups describe the symmetry operations present in an infinitely repeating three dimensional pattern (crystals are as an approximation to infinite repeating structures). Therefore each space group is a combination of the point group symmetry operations with translational (or space) symmetry operations.

A typical example of space group is $P 2_1/m$ –Where P is the type of Bravais lattice – Primitive in this example.

The letters following the P represent the symmetry operations which lie along a special direction in the crystal. In this example 2_1 represents a 2_1 screw axis in the direction of the unique axis of the monoclinic crystal system. The ‘/m’ represents an ordinary reflection plane which is perpendicular to the unique 2_1 axis.

The space groups and their associated symmetry operations are systematically detailed in the International Tables for Crystallography (Hahn, 1983).

In addition to the symmetry operations possessed by point groups there are two space symmetry operations which may be contained within space groups. These operations are termed glide planes and screw axes.

A screw axis is a combination of a rotation of $(360/n)$ followed by an appropriate translation parallel to the axis of rotation to preserve the translational repetition (where n is an integer). For example a 2_1 screw axis consists of a twofold rotation axis $(360^\circ/2)$ followed by a translation along half of the lattice axis that is parallel to the rotation Figure 3.8

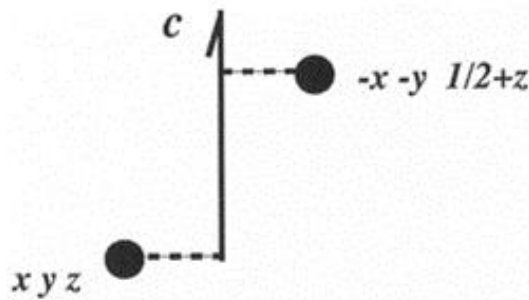


Figure 3.8. The effect a 2_1 screw axis has upon a particular point (Max Perutz et al., 1996).

A glide plane is a combination of a reflection in a mirror plane followed by a translation. There are five possible glide planes – denoted *a*, *b*, *c*, *n* and *d*. For example a *c* glide plane consists of a reflection in the *xy* plane followed by a translation along half of the *c* axis (Helmer, 1994).

Screw axes and glide planes can cause the systematic absence of certain reflections in a diffraction pattern. These systematic absences can help in the assignment of space groups as the absences are well known and are listed in the International Tables for Crystallography (although space group ambiguities do exist), while space group diagrams provide information as to the position of all symmetry operators within a unit cell (W. Clegg, 2005).

3.2.8. Bragg's Law

Shortly after the discovery of X-ray diffraction, William Henry Bragg and his son, William Lawrence Bragg, discovered that the geometry of the process is like to the reflection of light through a plane mirror (Bragg et al., 1983).. A consequence of the three-dimensional periodicity of a crystal structure is that perpendicular to certain directions it is possible to construct sets of many planes that are parallel with each other, equally spaced, and contain identical atomic arrangements. If an incident X-ray beam makes an angle θ with such a set of planes, the "reflected" beam also makes an angle θ with the planes, as in the case of optical reflection. It, of course, follows that the angle between the incident and reflected rays is 2θ .

Generally, the operation consists of the scattering of X-rays via the electron clouds surrounding the atoms of the crystal. The observed pattern is come from the constructive and destructive interference of the radiation scattered by all of the atoms, and the analogy to ordinary reflection is a result of the regularity of the atomic arrangement in a crystal.

Since there are large numbers of parallel planes involved in scattering X-rays, reflections from successive planes will interfere with each other, and there will be constructive interference only when the difference in path length between rays from successive planes is equal to a whole number of wavelengths. This is explained in Figure 3.7 where X-rays of wavelength λ are incident at angle θ on a set of planes with spacing d . and shows X-rays being diffracted from a series of parallel planes. In order for constructive interference, and hence diffraction to occur, the path difference ($AB+BC$) must equal an integral value of wavelengths (n) (W. Clegg et al., 2001).

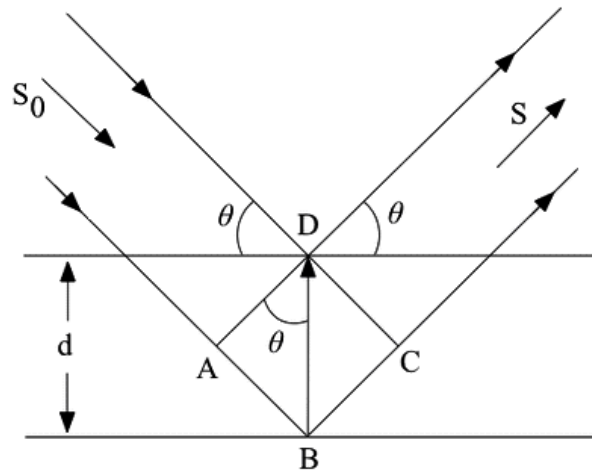


Figure 3.9. An X-ray beam makes angle θ with a set of planes with inter planar spacing d . For constructive interference $n\lambda = 2d\sin\theta$.

$$\text{If } AB + BC = n\lambda .$$

Where n is some integer.

From elementary geometry

$$AB = BC = d\sin\theta \quad \text{Eq.(3.1)}$$

Therefore,

$$2d\sin\theta = n\lambda . \quad \text{Eq.(3.2)}$$

And this is the well-known Bragg's law. Equation 3.2 provides no information other than that given by the Laue equations, but the interpretation of X-ray diffraction patterns is frequently easier in terms of Bragg's law since only one measured angle is required (Donald, 1975).

3.2.9. Miller Indices

Named after W. H. Miller these indices are an unambiguous way of defining crystal planes. They consist of three numbers (hkl) which correspond to the inverse of the ratio of the intercepts on the a , b and c axes of the unit cell for examples see Figures 3.10 & 3.11.

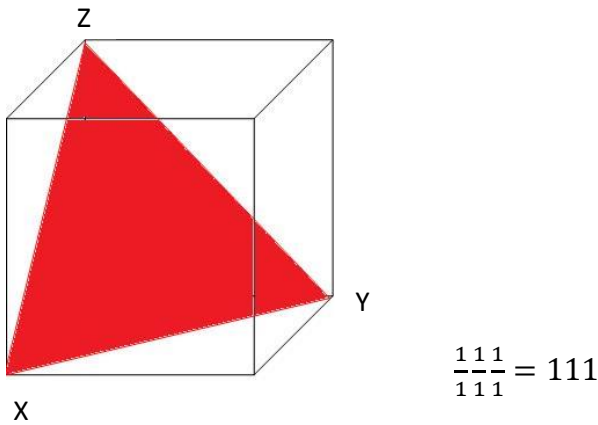


Figure 3.10. A pictorial representation of the 111 Miller plane.

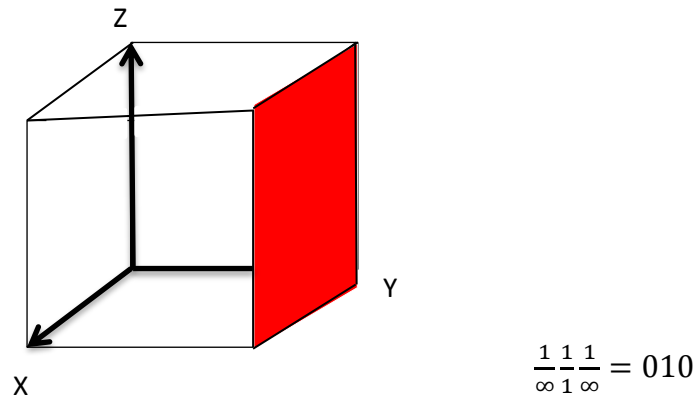


Figure 3.11. A pictorial representation of the 010 Miller plane.

3.2.10. The Reciprocal Lattice and Ewald Sphere

A single diffraction event (reflection) occurs when an entire set of parallel planes constructively interfere to create the diffracted X-ray beam. The use of constructs such as the reciprocal lattice and Ewald sphere aid in determining geometrically where the reflections will happen and satisfy Bragg's equation. The reciprocal lattice is related to the real crystal lattice axes (a, b, c) with axes a^* , b^* , c^* , such that a^* ($a^*=1/a$) is perpendicular to b and c , b^* ($b^*=1/b$) is perpendicular to a and c , and c^* ($c^*=1/c$) is perpendicular to a and b . Each reciprocal lattice point corresponds to a set of Miller

indices, hkl . Considering Bragg's equation, the diffraction angle θ is inversely related to the interplanar spacing d_{hkl} . This means that large unit cells will create small angles of diffraction, resulting in many reflections at a convenient angle from the incident beam. The opposite is true for small unit cells, which will produce fewer reflections. P.P.Ewald developed a construction of geometrical to help visualize which Bragg planes are in the correct direction to diffract. Corresponding to the Figure 3.12, the Ewald sphere has a radius equal to $1/\lambda$, with its center C . Points P , and O are on the sphere. As the crystal is rotated about point O , a reciprocal lattice point P occurs in relate with the circle. As incident X-rays passes through the crystal (line XO) at an angle θ , the reflected X-ray diverges from point C at angle 2θ through point P_{101} . The lines OP and BP are drawn; the length of OP (or 000 to 101) is $1/d_{hkl}$. The length of OB is $2/\lambda$, the diameter of the sphere. The angle BPO is equal to $\sin\theta$.

$$\sin \theta = OP/BO = (1/d_{hkl})/(2/\lambda) \quad \text{Eq. (3.3)}$$

Rearranged, this equation gives Bragg's law. The Ewald Sphere and the reciprocal lattice show that when a reciprocal lattice point falls on the sphere, a reflection will occur, thus Bragg's law is satisfied. Ewald's sphere shows which hkl planes are in the proper orientation to diffract, and how each reciprocal lattice point must be arranged with respect to the X-ray beam.

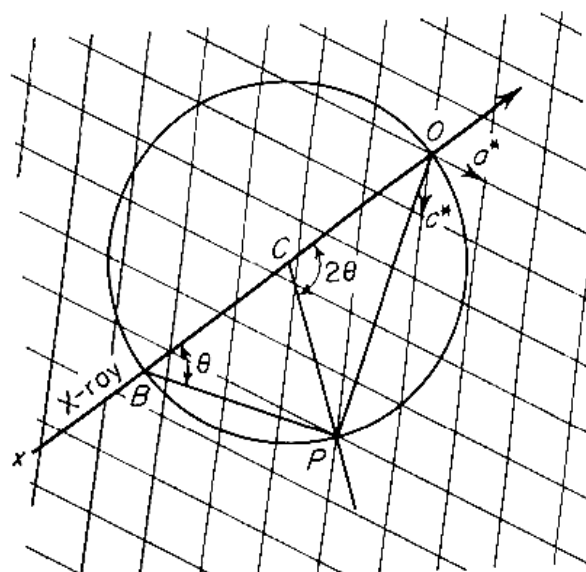


Figure 3.12. Diffraction in belongs to the reciprocal lattice.

3.2.11. The structure factor

The structure factor is the resultant of N waves scattered in the direction of the reflection hkl by the n atoms in the unit cell. Each of these waves has an amplitude proportional to f_j , the scattering factor of the atom and a phase σ_j with respect to the origin of the unit cell. Before the structure factor can be calculated, an expression for the phases in terms of the positions of the atoms and the indices of the reflection is needed. Such an expression can be derived by reference to Figure 3.11.

From the definition of the indices, the set of plane hkl cuts a into h , b into k , and c into l divisions. Since there is a phase difference of one cycle (2π radians, or 360°) between reflections from successive planes of any given set hkl , it is clear that the phase difference for unit translations along the axes or along any lines parallel to these axes $2\pi h$, $2\pi k$, and $2\pi l$ radians, respectively. For a fraction of a unit translation the phase difference will be that fraction of the phase difference for a unit translation.

In Figure 3.13 it can be seen that the phase difference in radians between the two points $0,0,0$ and x,y,z , for the set of planes hkl is the sum of the phase difference between the ends of vectors parallel to the axes and joining the two points. Thus if coordinates are expressed in fractions of a unit cell edge, the phase difference between 0 and $x,0,0$ is $(2\pi h)x$, that between $x,0,0$ and $x,y,0$ is $(2\pi k)y$, and that between $x,y,0$ and x,y,z is $(2\pi l)z$. Hence the total phase difference in radians between the origin and the point x,y,z is

$$\sigma = 2\pi(hx + ky + lz) \qquad \text{Eq. (3.4)}$$

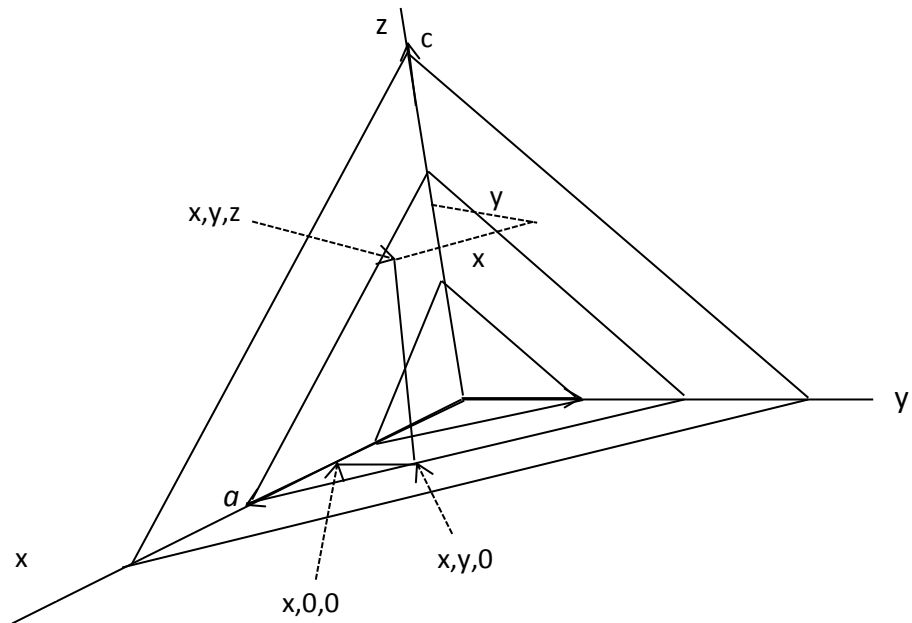


Figure 3.13. Axial components of the point x, y, z

Since the scattering factor of an atom is given in terms of an equivalent number of electrons, the structure factor likewise measured in electrons. The value calculated for the structure factor is that number of electron which if scattering in phase would show the same diffracting power as the actual set of electrons distributed throughout the unit cell (Lipson, 1966).

To determine the structure factor in exponential form we need the following equation

$$e^x = 1 + x + \frac{x^2}{2!} + \frac{x^3}{3!} + \dots \quad \text{Eq. (3.5)}$$

$$\cos x = 1 - \frac{x^2}{2!} + \frac{x^4}{4!} - \dots \quad \text{Eq. (3.6)}$$

$$\sin x = x - \frac{x^3}{3!} + \frac{x^5}{5!} + \dots \quad \text{Eq. (3.7)}$$

Substituting $x = i\sigma$ in the expression for the exponential, Eq. (3.5), and multiplying both sides of the equation by f , we have

$$f e^{i\sigma} = f \left(1 + i\sigma - \frac{\sigma^2}{2!} - \frac{\sigma^3}{3!} + \frac{\sigma^4}{4!} + \dots \right) \quad \text{Eq. (3.8)}$$

$$f e^{i\sigma} = f \left[1 - \frac{\sigma^2}{2!} + \frac{\sigma^4}{4!} + \dots + i \left(\sigma - \frac{\sigma^3}{3!} + \frac{\sigma^5}{5!} - \dots \right) \right] \quad \text{Eq. (3.9)}$$

$$\text{Or } f e^{i\sigma} = f(\cos \sigma + i \sin \sigma) \quad \text{Eq. (3.10)}$$

The right hand side of Eq. (3.10) is simply a complex number in polar form and represents a wave with amplitude f and phase angle σ . The left hand side of Eq. (3.10) is thus a compact representation for the structure factor:

$$F = \sum_j f_j e^{i\sigma_j} \quad \text{Eq. (3.11)}$$

Where f_j is, as previously, the scattering factor of the j th atom and σ_j phase with respect to the origin of the unit cell. Substituting in Eq. (3.11) the phase difference as given in Eq. (3.4),

$$F_{hkl} = \sum f_j e^{2\pi i(hx_j + ky_j + lz_j)} \quad \text{Eq. (3.12)}$$

This is the exponential form of the structure factor (Mellor et al., 1955).

Equation (3.12) represents the structure factor in a way that gives direct access to the three coordinates in direct space and the three indices in reciprocal space. A more compact, if less explicit, notation takes the three indices as characterizing a reciprocal space vector \mathbf{h} and the three coordinates as defining a direct space vector \mathbf{r} . the dot product of these two vectors is defined as

$$\mathbf{h} \cdot \mathbf{r} = hx + ky + lz \quad \text{Eq. (3.13)}$$

$$\text{So Eq. (3.12) can be written as: } F_{\mathbf{h}} = \sum f_j e^{2\pi i(\mathbf{h} \cdot \mathbf{r})} \quad \text{Eq. (3.14)}$$

This notation can be carried on to trigonometric expressions as well. Thus,

$$F_{\mathbf{h}} = \sum f_j \{ \cos 2\pi(\mathbf{h} \cdot \mathbf{r}) + i \sin 2\pi(\mathbf{h} \cdot \mathbf{r}) \} \quad \text{Eq. (3.15)}$$

We shall use this form where compactness is more important than explicit reference to the individual vector components.

3.3. X-rays and X-ray Generator

3.3.1 X-rays

The diffraction of X-rays by crystals was first demonstrated by Walther Friedrich, Paul Knipping and Max von Laue; seventeen years after Wilhelm Konrad Röntgen X-rays discovered in 1895. From their experimental X-ray diffraction on a copper sulphate crystal, they concluded that X-rays are electromagnetic radiation with wave lengths of the order 10^{-8} cm (a unit of length equivalent to Angstrom unit, 1Å) (Martin, 2003). X-rays having wave length of more than about 2Å are known as ‘soft’ X-rays. They are significantly absorbed through the air and strongly by water, and wave lengths of 0.2Å or less are very penetrating. The range of wave lengths between about 0.5Å and 1.6Å is the most suitable for X-ray crystallography. These waves are sufficiently penetrating to study samples up to a millimetre or so in size, but are scattered strongly by matter (Blow et al., 2002). X-ray crystallography is used extensively nowadays in the elucidation of crystal and molecular structures, the wide application of X-rays is shown in Figure 3.14.

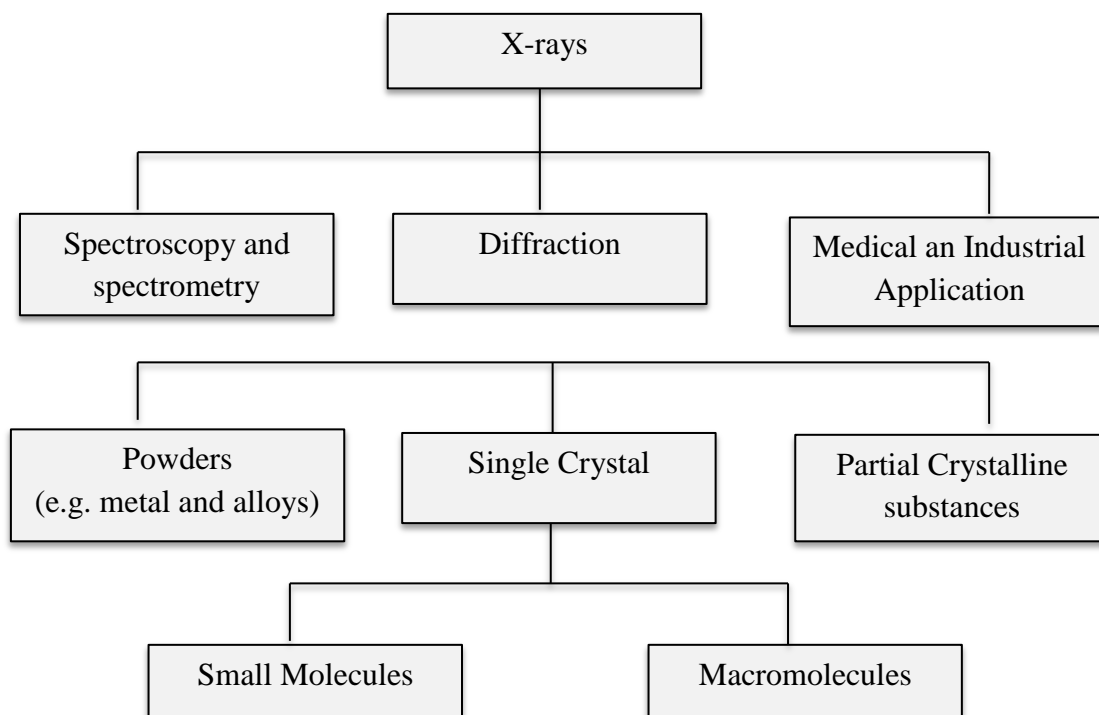


Figure 3.14. Schematic diagram for application of X-rays in modern science and technology (Lee et al., 1994).

3.3.2. Generation of X-rays

X-rays are a form of electromagnetic radiation which possess wavelengths within the range of 0.01 nm (0.1 Å) to 10 nm (100 Å) with wavelengths in the range 0.2 – 3 Å being useful in crystallography they are produced when accelerated electrons while penetrating through the target material and moving through the orbital electron cloud of atoms of the target are rapidly decelerated by the resistive force. Due to this deceleration of the bombarding electrons, their energy is emitted in the form of X-ray. This spectrum of X-ray radiation continuously varies in intensity from a lowest wavelength value known as short-wavelength limit. This radiation spectrum named as continuous or general radiation. When the accelerating potential for the bombarding electrons is increased, then these bombarding even after being decelerated still possess sufficient energy to knock off electrons from different orbits of the target atoms. When K-shell electrons are knocked off, then the target atoms are raised up to a potential energy corresponding to the K-shell. The electrons from the higher energy levels like L-shell or M-shell then jump down to the K-shell to fill up the vacancy and lower down the potential energy of the target atoms. These processes emit radiation of specific wavelengths which are characteristic of the target atom as they depend on the atomic number (Z) of the atoms of the target. These radiations being dependent on the atomic number are named as characteristic radiation (Sanat, 2008).

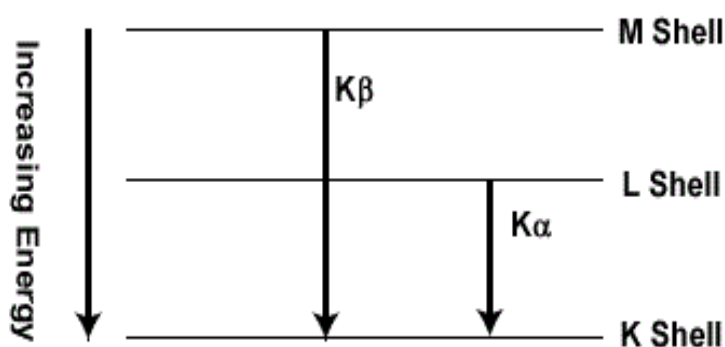


Figure 3.15. Emission of $K\alpha$ and $K\beta$.

X-ray consists of an electric field and magnetic field vector which are perpendicular to each other. These vectors oscillate in a sinusoidal manner perpendicular to the direction of propagation. Thus X-rays are the favoured form of

radiation in crystallography as they possess wavelengths comparable to bond lengths and can also be easily generated in a “home” laboratory setting. A more recent method of generating much more intense and finely tuneable X-rays using a synchrotron source is also now widely used.

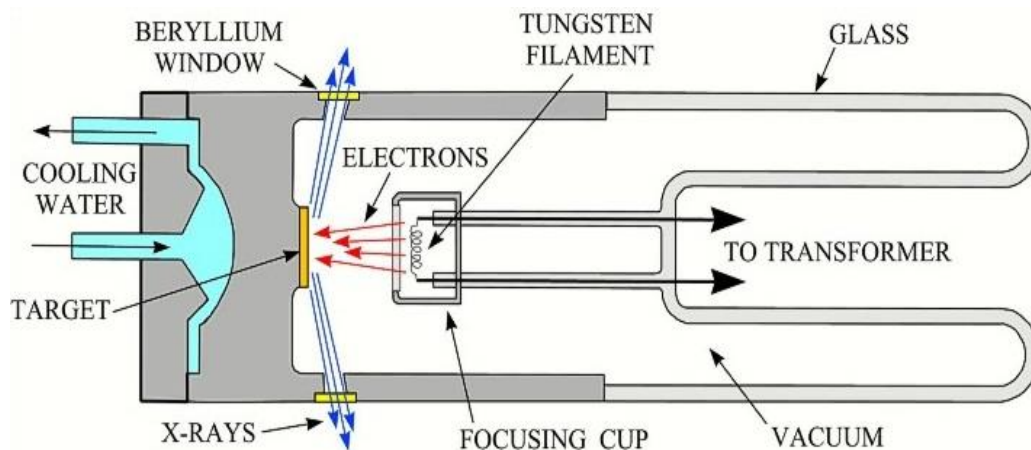


Figure 3.16. A schematic diagram of an X-ray tube (L.J. Poppe et al., 2001)

In Figure 3.16 the X-ray tubes used in modern day crystallography are known as filament (or Coolidge) tubes and date back to 1913. They consist of an evacuated glass enclosure which contains a tungsten filament and a disk of a target metal that responsible for the production of the characteristic wavelength of the X-rays. The most commonly used target metals are Molybdenum (wavelength = 0.71 \AA), Copper (1.54 \AA) and Silver (0.56 \AA).

To initiate the production of X-rays the tungsten filament is heated by passing an electric current through it. This results in the production of electrons which are accelerated by a potential difference and directed towards the target metal. If the potential difference is sufficiently high (typically 50kV) the electrons will possess enough energy to cause ionisation of inner core electron's of the target metal. To compensate an electron in a higher atomic energy level for the metal will drop in energy to take the place of the ejected electron. This results in the emission of a photon with a characteristic wavelength. The characteristic wavelength produced is dependent upon the metal atom energy levels from which each electron is ejected. For example M_oK_α emission corresponds to electrons moving between the L and M shells ($\lambda = 0.71\text{\AA}$) of

Molybdenum whilst M_oK_β emission corresponds to a movement between the L and K shells ($\lambda = 0.63\lambda$).

This characteristic wavelength created is defined by Equation (3.16).

$$\lambda = \frac{hc}{E_1 - E_2} \quad \text{Eq(3.16)}$$

Where :

- h = Planck constant (6.6261×10^{-34} J s)
- c = Speed of light (2.9989×10^8 m/s)
- E_1 = Lower energy level of target atom
- E_2 = Higher energy level of target atom

The spectra purity of the X-ray beam onto the crystal is created by using filters to remove background and other unwanted wavelengths whilst a beryllium window allows the X-rays to leave the tube head with minimum absorption.

This method of X-ray production can be considered quite inefficient as the vast majority of the energy carried by the electrons is converted into heat rather than X-rays (literature sources mention 1% X-ray conversion⁸). The heating of the target is largely compensated by a water cooling system which prevents melting of the target material up to certain current limits. An additional disadvantage of this method is that the X-rays generated are quite divergent which may pose a problem if small crystals are under study.

An improved method of generating X-rays in the home laboratory is known as a rotating anode. In this apparatus the target metal is cylindrical and is spun about its axis. This allows the energy of the X-rays to be spread out over a larger overall area thereby reducing the heating problem. As a result much higher electrical currents can be introduced which creates a much higher flux density. This method of X-ray generation is important especially for molecules which possess large unit cells such as proteins which are often in large complexes.

3.3.3. Synchrotron source X-ray generation

Synchrotrons were initially developed as a tool in particle physics to accelerate beta particles (electrons and positrons). It is observed that when such particles are accelerated through magnetic fields at relativistic speeds they lose energy in the form of electromagnetic radiation (this radiation covers the entire EM spectrum not just X-rays).

When the beta particles pass through the magnetic fields they change direction. This causes the tangential emission of radiation. Although emission of radiation occurs at non relativistic speeds, a feature of relativity known as the Lorentz transformation means that the radiation is emitted in a highly collimated fashion at speeds approaching that of the speed of light. This emission of radiation was first observed in 1946 at a 70MeV synchrotron in Schenectady by F. R. Elder et al (Elder et al., 1947). Today many synchrotron sources are now operational as nationally and internationally shared facilities.

Synchrotrons consist of a linear accelerator (LINAC) which creates high energy electrons (around 10MeV). These electrons are subsequently injected into a small accelerator (known as a booster synchrotron) which increases the energy of the electrons to around 500MeV. Once this point has been reached the electrons are injected into the main synchrotron ring where the energy is further increased via multiple passes through radio frequency cavities. This produces X-rays which extends to the necessary short wavelengths and are much more intense and well collimated than laboratory based sources. This allows for extremely fast data collection times and smaller crystals to be studied. The continuous spectrum allows for the fine tuning of the selected wavelengths using monochromators. Alternatively the whole 'white' X-ray spectrum may be used in Laue diffraction experiments

3.3.4. X-ray Detectors

The diffracted beams intensities are measured by intercepting the beams with something which has a sensitivity to X-rays. X-ray detectors respond to the energy of the diffracted beam, called intensity, which (at a given wave length) is proportional to the number of photons it delivers. Nowadays the diffracted spots are usually recorded

on image plates rather than on X-ray films, the classical method, or by an electronic detector. Electronic area detectors feed the signals they detect directly in a digitized form into a computer, hence its name. Various forms of X-ray detectors can be available; some may count single photons, some providing only measurements of count rate or total flux, others measuring the energy, position, and incidence time of each X-ray. Among the numerous types of area detectors which are currently used, we shall concentrate on the two most popular types namely:

- The charge-coupled devices (CCD)
- The image plate (IP).

These two types of device fulfil some of the most important requirements for X-ray area detectors, such as high detective quantum efficiency (DQE), wide dynamic range, linearity of response, high spatial resolution, large active area, uniformity of response, and high count-rate capability.

The IP is a plastic plate, possibly flexible, which is coated with small crystals of photo-stimulable phosphors embedded in an organic binder. The photo-stimulable phosphor stores a fraction of the absorbed X-ray energy. In a second step, when the IP is activated by visible light, it emits photo-stimulated luminescence (PSL) which is proportional to the absorbed X-ray intensity. The PSL is then collected by high-quantum-efficiency photomultiplier tube (PMT) and converted to a digital image which can be further processed. The residual image on the IP can be completely erased by illumination with visible light in order to be ready for the next measurement.

The DQE, defined as the square of signal-to-noise ratio of the input over the square of the signal-to-noise ratio of the output, exhibits excellent performance in comparison with any other detectors. The dynamic range of the IP is of the order of $1:10^5$. The amplitude of the IP signal per X-ray photon depends on the energy of the X-ray photon. Therefore, when different energies of X-rays are recorded in the IP, in Laue diffraction for example, the IP must be calibrated (Ted Janssen et al., 2007).

The CCD is another type of area detector which has been widely accepted as detectors for collecting X-ray diffraction images for both macromolecules and small-

molecule crystals, including this work. In general, they consist of several components: as energy converter, mostly phosphor; an optical relay with fibre optics taper, and the imaging CCD (Muchmore et al., 1999). The input signal is transformed several times while crossing the sequence of stages.

These detectors have the advantage of being able to record a number of diffracted beams at the simultaneously, thereby reducing data collection times. A CCD detector employs a semiconductor in which the incident X-rays induce the production of free electrons and electron holes (Clegg et al., 2009). The electrons produced are trapped in potential wells, and in addition to the electron holes, are read out as a current. The magnitude of this current is proportional to the intensity of the diffracted beams. The various designs of CCD detectors can be roughly divided into two groups depending on how the intensity of the radiation is detected. This may be done by either measuring the intensity of the X-rays directly or by conversion of the X-rays to visible light using a phosphor conversion mechanism (Helliwell, et al., 1992).

Diffractometers that utilise a CCD detector are often known as three circle diffractometers. This is because they possess three rotation axes (one in relation to the detector and two in relation to the crystal). Scintillation counter based diffractometers possess four rotation axes as the detector is smaller and can only record reflections which occur in the horizontal plane. As a result an additional crystal rotation axes is required. (Ted Janssen et al., 2007).

3.3.5. The goniometer

In crystallography, ‘goniometer’ denotes all the gears required to position and rotate a crystal in the X-ray beam through data collection. The simplest systems are produce a rotation about three or four axes. In four-circle diffractometer, a crystal can be rotated around three axes (χ , ϕ and ω) independently, and the detector can be rotated around a fourth angle (2θ , concentric with ω), which give this the name ‘four-circle diffractometer. The 2θ and ω angles are measured relative to the rotation of the detector (corresponds to the Braggs angle for angular spread), and rotation of the base of the goniometer head, respectively. The χ and ϕ angles are measured due to rotation of the

goniometer head around its own axis and rotation of the ϕ -axis relative to the reflection plane, respectively. For example, the Kappa apex II goniometer features the Kappa 4-axis goniometer where it uses a horizontally oriented Kappa goniometer with $2\theta, \omega$, kappa (κ) and ϕ drives while the SMART APEX II goniometer (Figure 3.17), the three-circle instrument uses a horizontally oriented D8 goniometer base with $2\theta, \omega$ and ϕ drives. This three-axis system incorporates a fixed chi stage with χ angle of 54.74° and a ϕ drive with 360° rotation, which is so compact that it swings into the incident beam collimator, allowing free rotation in ω .

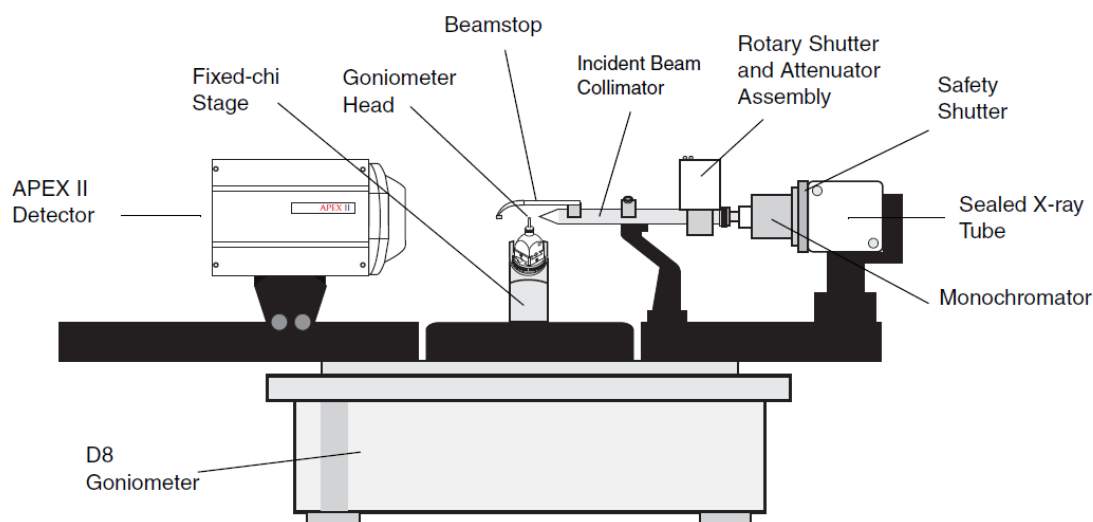


Figure 3.17. SMART APEXII goniometer elements-adapted from (Bruker advanced X-ray solutions- APEXII user manual version 1.22)

3.3.5.1. Goniometer head

A goniometer head is a device allowing the crystallographer to put the crystal in the center of the beam, and perhaps to orient it. It has various possible adjustments (height, and X and Y adjustments or lateral adjustments) which are used to center the crystal in the crosswire of video microscope and in the X-ray beam so that a crystal can be bathed in a radiation. Also it has a brass rod which holds glass fiber, this is used to mount a crystal on it (User Manual, 2006)

3.4. Single Crystal X-ray Diffraction

3.4.1. Introduction

Structure determines function” is an axiom which emphasizes the connection between how a molecular system functions and its natural structure. The essential objective of X-ray crystallography is to get knowledge of the molecular structures of natural and synthesized compounds. It gives the three-dimensional structures of new and existing crystalline materials, which can be utilized to predict or explain functional information. More specifically, X-ray crystallography detects what atoms are present and their positions, distances and angles between atoms, and the symmetry involved that produces the entire crystalline substance. Single-crystal structure determination has become an important and extremely powerful tool, not only for mineralogists, inorganic and structural chemists, but also for many other scientists who are interested in the structural basis for the properties of chemical and biological systems at the molecular level (Glusker et al., 1995).

Single-crystal X-ray structure determination may also be considered as the ultimate analytical tool, because it provides direct, unequivocal identification of the sample under investigation. Unlike many spectroscopic techniques, a successful X-ray structure determination yields the precise composition of the unit cell, including the identity and position of all atoms.

Except in exceptional cases, only the correct molecular structure will make a good fit to the observed X-ray diffraction intensities, and all incorrect structures make fits that are clearly inferior.

A number of other experimental techniques may also provide useful structural information, but they are often limited in the amount of information or resolution they can provide, or suffer from other limitations. Electron diffraction and microwave spectroscopy can provide very exact structural data for molecules in the gas phase. Other forms of spectroscopy, containing Extended X-ray Absorption Fine Structure (EXAFS) and Resonance Raman spectroscopy provide only limited information about

the environment of a small number of atoms, bonds, or functional groups, mostly of elements having atomic numbers greater than oxygen (Cullity et al., 1978)

Libraries of spectra are useful in identifying compounds and commonly known functional groups. However, this practice may be not useful in the investigation of newly synthesized compounds not found in spectral libraries. Techniques for the direct visualization of molecules, like atomic force microscopy, in which a probe is scanned over molecular surface, do not provide details of the molecular interior.

Over the past few decades, many technological improvements have been directed to optimizing X-ray diffraction instruments and software programs, so that the once long, arduous task of structure determination has evolved into a fairly straightforward analytical technique. Single-crystal analysis varies from other diffraction methods because the measurement of a diffraction pattern is determined in three dimensions, and produced from an oriented single crystal (Müller et al., 2005).

Single crystal X-ray diffraction has become a routine analytical tool used to determine the solid state molecular structure of compounds. With the help of modern technological advances data collection times have been reduced from weeks to hours over the last couple of decades by the invention of area detectors. The information that can be obtained from these experiments is extremely valuable. Not only does it provide a 3D model of the structure under investigation, the technique also provides information on configuration, conformation, torsion and bond angles, bond lengths and bonding interactions. A brief description of the technique is described in the following section.

3.4.2. Experimental Set-up

The schematic in figure 2.8 illustrates the standard set-up used for single crystal X-ray structure determination experiments. X-rays are generated by firing high speed electrons at a metal target, which is typically made out of copper or molybdenum. Molybdenum is the most popular target material for single-crystal diffraction, with MoK_{α} radiation = 0.7107 Å. The crystal is mounted on a fine glass fibre fixed on a goniometer head which can rotate during data collection. X-rays are fired toward the crystal where some are diffracted and recorded as a series of diffraction spots by the

detector (each spot corresponds to diffraction from a set of Miller planes for which Bragg's law has been satisfied). A beam stop is located directly opposite the collimator to block transmitted rays and prevent burn-out of the detector. Reflected rays are not picked up by the detector due to the angles involved. Diffracted rays at the correct orientation for the configuration are then collected by the detector (Putnis et al., 1992).

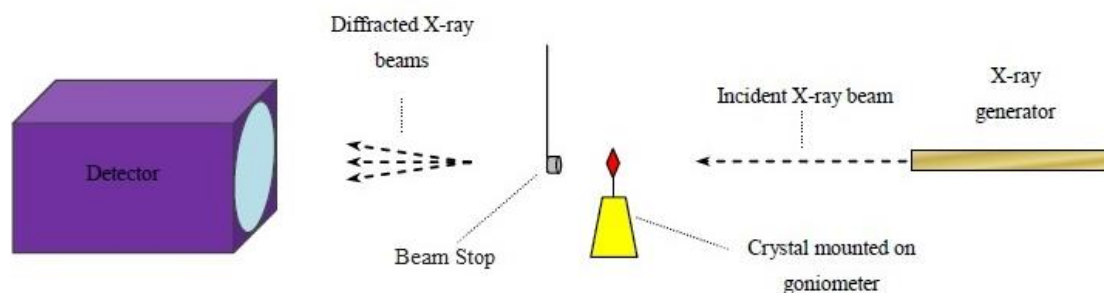


Figure 3.18. Schematic illustrating set-up for a single crystal X-ray diffraction experiment.

3.4.3. Data Collection Strategy

The experiment consists of the collection of reflections as reciprocal lattice points pass through the sphere of reflection. The aim of data collection is to collect as many reflections as possible in order to find the unique electron distribution in the unit cell that produces a calculated diffraction pattern that matches the observed intensities as closely as possible. The analysis is often simplified by the existence of symmetry in the unit cell. This decreases the problem to finding the density in the asymmetric unit only. The total electron density of the unit cell is then produced by the space-group symmetry operations, which can be deduced from the diffraction symmetry. In summary, X-rays will be scattered by crystals in discrete directions only. The location determinations of these directions are being by the orientation of the crystal, the unit cell dimensions, and the wavelength of the X-rays (Clark et al., 2007).

The needed components for the experiment are a crystal, a detector, an X-ray source with shutter, and a goniometer to orient and rotate the crystal. The SMART program controls the detector, the goniometer, and the shutter to make a series of

picture (frames) at specified goniometer setting angles. Each exposure is created by a simultaneous opening of the shutter and the rotation of the crystal by a small degree.

At the end of the exposure, the shutter closes, the integrated counts collected in the detector are transported to computer memory or hard disk to processing later, and the detector memory is cleared. The cycle is then regained for the next image (picture).

It is necessary to synchronize the shutter with the crystal rotation so that adjacent images truly reflect adjacent portions of reciprocal space. The detector should be positioned so that its entire active area is used, then diffraction spots do not overlap and the highest possible resolution is obtained.

Generally detectors do not have a regular response over the entire active area. They also will distort the diffraction pattern in some geometric method. Locational distortions and inhomogeneity of response must be corrected and defective pixels flagged, so that pixels can be mapped accurately to the actual location. Non uniformity of response might arise with a detector because of differentiation in phosphor thickness, fiber-optic taper properties, pixel area, paths through windows, and so other.

3.4.4. Device Information

At the University of Dicle, Science and Technology Application and Research Center has the state-of-the art instrumentation for single crystal structure determination. The Bruker APEX SMART CCD diffractometer system is equipped with a Breeze CCD detector, which has features for getting quality data sets in a fraction of the time required by instruments without CCD detectors. A pixel size the Bruker CCD detector is 120 microns and contains 512 X 512 pixels. Physically, the SMART detector sub system made up of four components in addition to the PC utilized to run the SMART data collection program. Provided is an image of the detector system. First is the detector itself and mounted on the goniometer dovetail. Next is the CEU (Camera Electronics Unit). The CEU digitizes the analog signal from the detector which controls detector gain, exposure times, and other parameters under direction of the computer. Third is the PC interface card, and located in the PC and connects the PC to the CEU. Fourth is the refrigeration device that cools the CCD to its operating temperature.

The SMART APEX system, consists of the following basic components (User manual, 2001)

- APEX CCD detector
- 3 axis SMART goniometer
- X-rya generator
- Radiation safety enclosure with interlocks and warning lights
- Refrigerated recirculator for the detector
- Instrument control (BIS) and crystallographic software (APEX 2) computer
- Video microscope

Figure 3.19 shows some components of SMART APEX system

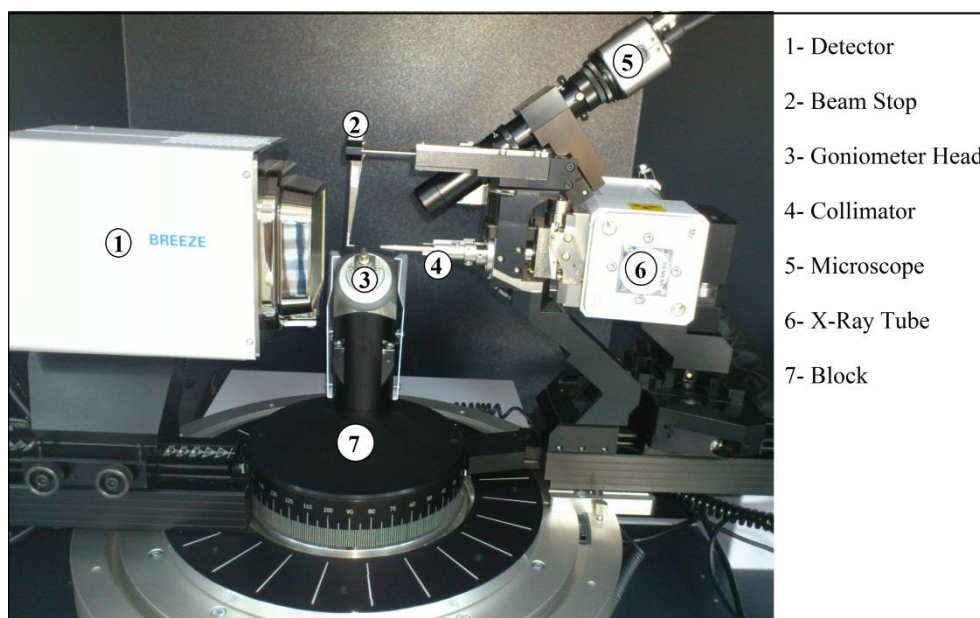


Figure 3.19. some components of SMART APEX system

3.4.5. Structure Solution

Once crystals of a suitable size have been grown the crystal structure determination procedure can begin. This procedure can be thought of as being divided into three main stages –

- The first stage involves the measurement of the intensities of the Bragg reflections and the application of corrections to take into account various geometrical and physical phenomena.

- The second stage involves using mathematical and computer program methods to imitate the behaviour of a microscope lens to solve the phase problem.
- The final stage involves refining the initial structure so that there is an optimum agreement between the observed and calculated structure factors.

The steps involved in each of these stages are further explained below.

3.4.5.1. Stage 1 – Measurement of X-ray intensities

3.4.5.1.1. Step 1 - The first step towards measuring X-ray intensities is the selection and preparation of a suitable single crystal

For use in home laboratory experiments single crystals in the order of 0.2-0.5 mm are routinely required. This is because the X-ray beam generated is relatively weak in intensity (compared to a synchrotron source) and the diameter is less than 1 mm; using such a small size ensures that the crystal is fully immersed in the X-ray beam. It is important to inspect crystals beforehand using a microscope to ensure that no visible defects such as cracks or twinning are apparent. In addition crossed polarisers can be used to ensure that the crystals extinguish. This can help to reveal defects within the crystal that were previously not apparent. However should not be considered a conclusive test as some crystals (depending upon their symmetry) do not extinguish.

Once a crystal of a suitable size and quality has been selected it can be fixed on the tip of a thin glass fibre using epoxy or cement, or in a loop including specific oil (Figure 3.20) It is necessary to know the stability properties of the crystals. Crystals can be sensitive to light, air or wetness, or susceptible to loss of crystallisation solvent. If so, a special treatment is required. For example, they can be mounted inside sealed glass capillaries or the data collection can be performed at low temperature.

Finally, the selected crystal is mounted onto a goniometer head and placed onto the diffractometer. The goniometer head is a device that allows the crystal to be easily centred in the X-ray beam. Additionally in modern day diffractometers a high magnification video camera is used to ensure that the crystal is in the correct position and to record a digital picture of the crystal for size determination.

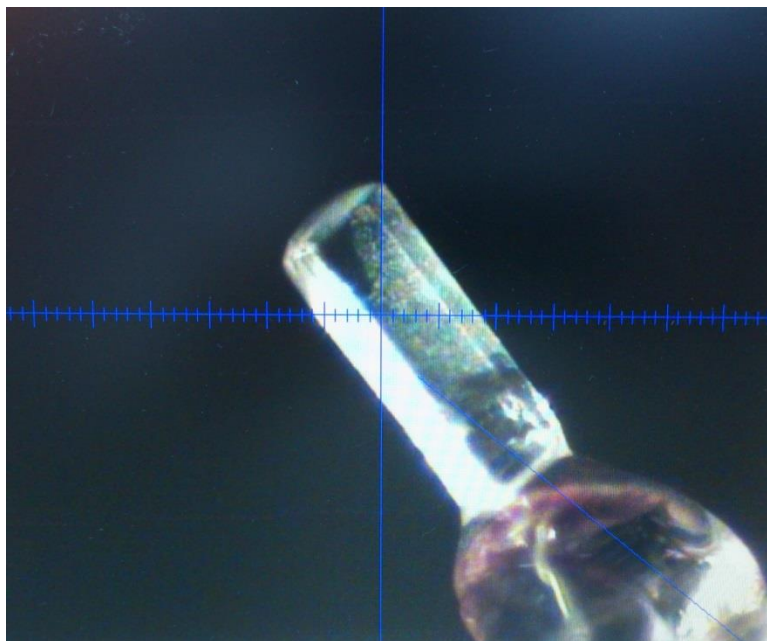


Figure 3.20. A crystal mounted on the tip using epoxy. Pictures via a high magnification video camera present on the diffractometer.

3.4.5.1.2. Step 2 – The collection of the X-ray intensities

Once the crystal has been correctly centred with respect to the X-ray beam irradiation can begin. This irradiation will produce a diffraction pattern that is commonly recorded by a CCD detector. The CCD diffraction images collected then need to be integrated to produce a list of reflections i.e. spots (hkl values) each with an associated intensity.

It is possible to determine the unit cell dimensions from the first few images. Other factors such as the quality of the crystal (the mosaic spread and/or splitting) are also obvious from the first few images obtained.

3.4.5.1.3. Step 3 – The diffraction images data reduction process

This step includes the application of corrections to the measured intensities which take into account various geometrical and physical phenomena. A common geometrical correction applied is known as the Lorentz-polarisation factor.

The Lorentz factor is related to the amount of time the reflection is in a diffraction position and is instrument dependent. The polarisation factor is required because the reflected X-rays are partially polarised.

A commonly applied physical correction concerns the absorption of X-rays by crystals (this is particularly true for inorganic crystals). Absorption corrections are needed for crystals that are not approximately spherical and are calculated by analysing systematic variations in the intensities of symmetry related reflections. This is because the amount of absorption is dependent upon the path length the X-rays travel through the crystal.

Absorption of X-rays also increases the larger the crystal is; using a crystal as small as possible helps to minimise this error. Finally absorption varies with elemental composition; often heavy atoms strongly absorb X-rays.

The data reduction process also involves the merging of symmetry related reflections and the calculation and application of scale factors to the measured reflections. The result is a unique, scaled data set. The data reduction process is a 'black box' method that is performed by computers.

3.4.5.2. Stage 2 – The crystallographic phase problem and possible solutions

The phase problem is intrinsic to X-ray crystallography. Each of the diffracted X-rays will have a particular phase and amplitude associated with it. X-ray sensitive detection methods such as photographic film or CCD detectors are able to measure intensities from which the amplitudes are easily obtained (intensities = amplitude²).

However the relative phases of the waves are lost during the experiment. This is a problem because in order to elucidate the crystal structure both the intensities and relative phases are required. Therefore a method of obtaining approximate phases and hence solving the phase problem is required. In small molecule crystallography two methods are almost exclusively used which both utilise a branch of mathematics known as Fourier series.

Fourier series arise from Fourier's theorem which states that any periodic function can be represented by a summation of *sin* and *cosin* terms. The diffraction pattern and the electron density of a crystal are related by a Fourier series. In addition a diffraction pattern consists of well defined individual spots. Therefore a summation must be used as opposed to integration which would be performed if the pattern was

diffuse. Crystals can be described by a Fourier series as the structure of a crystal is a periodically repeating, (effectively) infinite array.

The structure factor equation is used to describe how the incident X-rays are diffracted by the constituent atoms of a crystal. This equation takes into account the scattering power of each atom (which is described by f_j which is the scattering factor for the j^{th} atom) and is dependent upon electron density. This is described by previous Equation (3.12) written as :

$$F(hkl) = \sum_{j=1}^N f_j e^{2\pi i(hx_j + ky_j + lz_j)}$$

Where:

- N = The number of atoms within the structure
- f_j = Atomic scattering factor for the j^{th} atom

The electron density calculation must be performed in three dimensions in order for a three dimensional structure to be produced. The unit cell volume (V) must also be taken into account. The equation used to calculate the electron density at a particular point (xyz) is given by Equation 3.17.

$$\rho(x, y, z) = \frac{1}{V} \sum_{h,k,l} |F(h, k, l)| e^{-2\pi i(hx + ky + lz)} \quad \text{Eq. (3.17)}$$

The two commonly used methods used to solve the phase problem in small molecule crystallography are described below.

3.4.5.2.1 Patterson Methods

This method is commonly employed when there is one or a small number of heavy atoms present in the structure. In 1934 A. L. Patterson presented a synthesis (or Patterson map) that is obtained by performing a Fourier series on the square of the amplitudes with all waves taken in phase. If there are an N number of atoms in a unit cell then there is a N^2 number of vectors running between these atoms. Therefore a Patterson map shows where atoms are located relative to each other but not where they are located with respect to the unit cell origin. The result is a map that has an

appearance similar to that of an electron density map in that it contains peaks of positive density located in particular positions. However this is not a map of electron density, instead it is a map of the vectors between pairs of atoms in the structure (Patterson et al., 1935). The Patterson synthesis is described mathematically by Equation 3.18.

$$p(x, y, z) = \frac{1}{V} \sum_{h,k,l}^{+\infty}_{-\infty} |F_o(h, k, l)|^2 e^{-2\pi i(hxj+kyj+lzj)} \quad \text{Eq. (3.18)}$$

Where V = The unit cell volume (in m³).

3.4.5.2.2 Direct Methods

This method was developed for equal atom structures i.e. those that contain no heavy atoms.

Direct methods also use the measured intensities but takes advantage of the fact that electron density within a crystal cannot be negative. This places restrictions on the possible phase angles between reflections. The process is almost a trial and error approach – the reflections which contribute most to the Fourier transform are selected as are approximations that appear promising (assessed by a numerical factor). The Fourier series are calculated using the measured intensities and these approximate phases. Sensible looking chemical fragments can be used to assess the different trial structures. The resulting trial structure is only an initial approximation of the true structure and must undergo further refinement.

Direct methods are often described as black box as the process is automated and performed by computers.

3.4.5.3 Stage 3 - Structure Refinement

The final stage involves refining the initial structure so that there is an optimum agreement between the observed structure factor amplitudes and the structure factor amplitudes calculated for the current structure.

The measure by which these factors agree is described by the conventional residual factor (commonly known as the *R* factor). The *R* factor is defined by Equation 3.19.

$$R = \frac{\sum_{2\theta i} |y_o(2\theta i) - y_c(2\theta i)|}{\sum_{2\theta i} |y_o(2\theta i)|} \quad \text{Eq.(3.19)}$$

Where

y_o = Observed structure factor amplitude

y_c = Calculated structure factor amplitude from model

As illustrated by equation above the lower the R factor the better the agreement and the more correct the structure is. That the earlier stages of the structure determination procedure were performed correctly is essential if a low R factor is to be obtained.

Refinement uses a mathematical technique known as least squares analysis which adjusts

parameters such as atom positions and atomic displacement parameters in order to produce the maximum agreement between two sets of data (in this case the observed and calculated amplitudes). The refinement on F2 was used in this thesis and is defined by Equation 3.20.

$$\sum w(F_o^2 - F_c^2) \quad \text{Eq.(3.20)}$$

Where

F_o = Observed structure factor amplitude

F_c = Calculated structure factor amplitude from model

Several cycles of refinement are required as the data used is calculated using Fourier series which are nonlinear equations. Consequently cycles of refinement are required until the adjustments of the parameters are insignificant (a process known as convergence).

The refinement parameters can be split into two groups based on the mathematical detail used to describe the atoms. Isotropic refinement uses three positional coordinates (x, y, z) as well as a single vibrational parameter to approximate vibrating atoms as spheres. Anisotropic refinement uses the same three positional coordinates as well as six vibrational parameters to describe atoms in terms of ellipsoids. Although a perfect ellipsoid can be described by three vibrational parameters atoms typically possess distorted ellipsoids which are described by require six vibrational parameters. This results in a significantly more accurate and realistic model

structure. In addition, once anisotropic refinement has been carried out small peaks can often be observed, corresponding to hydrogen atom positions.

The process of refinement is complete when convergence is achieved and the electron density map contains no undefined peaks or holes.

For small molecule X-ray crystallography a final R factor in the range 0.02 – 0.07 is an indicator of a good quality structure.

4. FINDING AND DISCUSSION

4.1. Overview

In this chapter mainly focuses brief explanations on: the experimental results, data collection and structure solution, structure refinement, and structure conformation discussion of the two compounds.

4.2. Compound I: Dichloro[1,3-bis-(2-ethoxybenzyl)benzimidazole-2-ylidene]pyridine palladium(II)

Single crystal X-ray diffraction measurements were made on a yellow prism shaped crystal of $C_{30}H_{31}Cl_2N_3O_2Pd$ with 0.45x0.30x0.15 mm at 296(2) K on a Bruker AXS SMART diffractometer.

The crystal was centred using rotating screws on the goniometer head and a video camera as a visual aide. Firstly the x-axis was adjusted at phi 0° to ensure the crystal was centred. Once complete the screw was rotated to phi 180° and the crystal centred again. This process was repeated in the same manner for the y-axis but with phi angles 90° and 270°. Once the crystal was completely centred it was irradiated with monochromated MoK α radiation. The X-ray generator settings were 50kV and 50 mA.

The computer program SAINT(SAINT-Plus, 2007) was used to collect and integrate the CCD frame images in order to produce integrated intensities. This produced files with filename extensions .p4p and .RAW. These files were then introduced into SHELX XPREP (Sheldrick et al., 1997) for determination of the crystal system and space group. SHELX SADABS was used to produce an absorption corrected data set which took into account absorption of X-rays by the crystal, although this was a symmetrically sized crystal (crystal dimensions listed in Table 4.1). The patterson methods program SHELX XS was used to solve the structure with further refinement being performed in the SHELX program

Full-matrix least-square refinement on F^2 against all reflections was carried out by SHELXTL (Sheldrick, 2008) All non-hydrogen heavy atoms were refined anisotropically, complete crystal data are given in Table 4.1.

All the hydrogen atoms in the molecule were identified from the difference electron density map, further idealized and treated as riding with a distance $d(\text{C-H})=0.93\text{\AA}$ (for aromatic C-H), $d(\text{C-H})=0.97\text{\AA}$ for (CH_2) and $d(\text{C-H})=0.96\text{\AA}$ for (CH_3) respectively. In all cases $U_{\text{iso}}(\text{H})=1.2U_{\text{eq}}$.

The solid state molecular structure can be seen in Figure 4.1. and selected bond distances and angles are listed in Table 4.2. and Table 4.3.

Table 4.1. Summary of crystallographic data for compound (I)

Empirical Formula	C₃₀H₃₁Cl₂N₃O₂Pd		
Chemical Formula Weight	642.88		
Crystal System	Tetragonal		
Space Group	P 4 ₁ 2 ₁ 2		
Wavelength (Å)	MoKα 0.71073		
a (Å)	12.4519(3)	α (°)	90
b (Å)	12.4519	β (°)	90
c (Å)	19.0440(4)	γ (°)	90
Volume (Å³)	2952.77(1)		
Z	4		
F (000)	1312		
Crystal size	0.45x0.30x0.15		
Absorption correction	Multi-scan		
Theta (θ) range (θ_{min} - θ_{max})	2.5° → 34.1°		
Index ranges	h = -19→19, k = -19→19, l = -22→29		
Reflection collected	46895		
Independent reflections	5776		
observed reflections (I>2σ(I))	4952		
Refinement method	Full-matrix least-squares on F ²		
Data/restraints/parameter	5776/0/190		
Peak differences in electron density map	Δρ _{max} = 0.366 eÅ ⁻³ , Δρ _{min} = -0.226 eÅ ⁻³		
Absorption Coefficient (mm⁻¹)	0.840		
R_{int}	0.0393		
R₁, wR₂	0.034, 0.049		
R indices (all data)	0.0345		
Goodness of fit S	1.028		
Temperature (K)	296(2)		

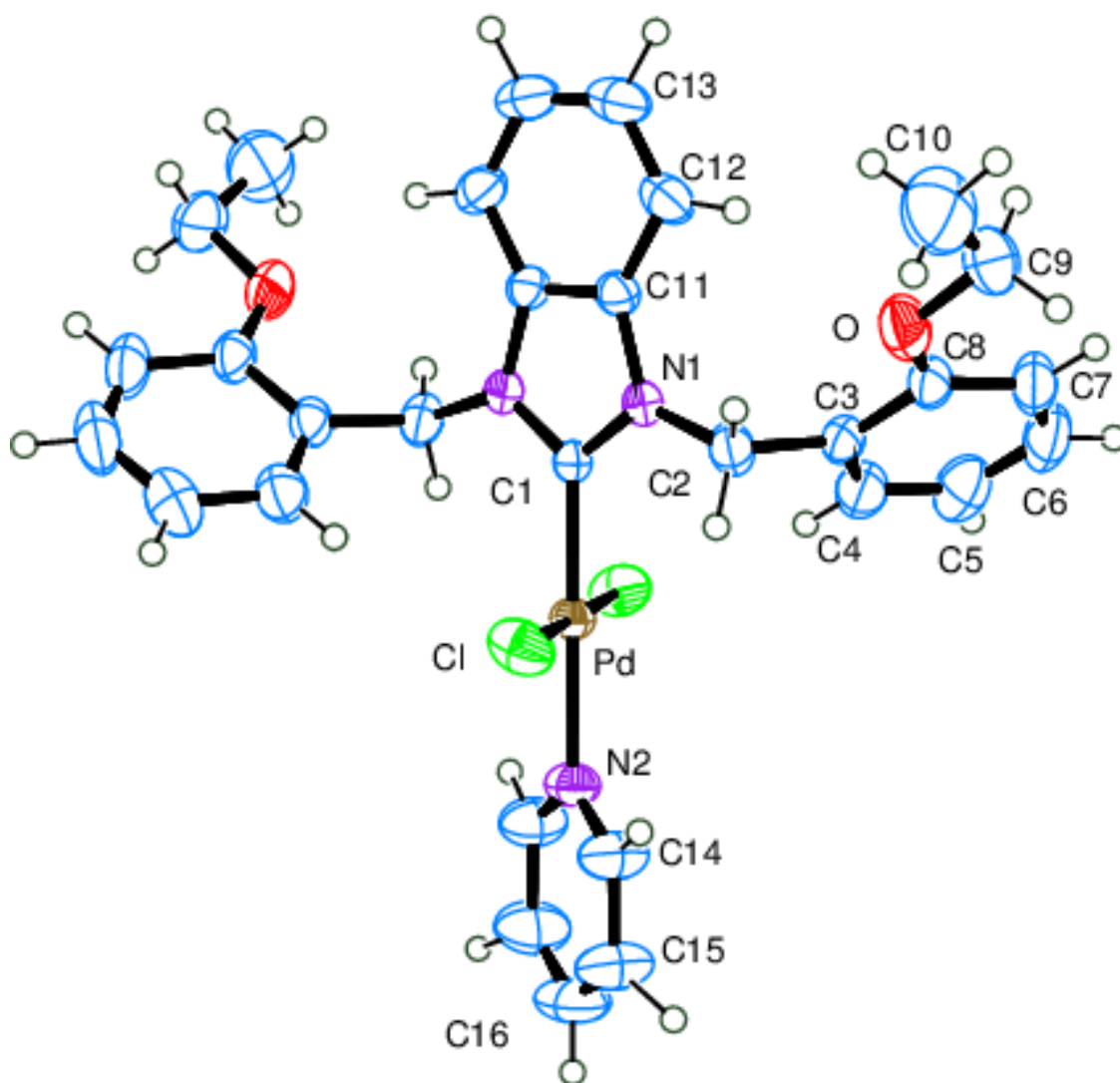


Figure 4.1. Molecular structure of Compound (I) (Dichloro-[1,3-bis-(2-etoksibenzil)benzimidazole-2-yliden] pyridine palladium (II)) (ORTEP diagram)

The central Palladium atom is bonded to Cl, Cla, N, and C atoms. The coordination geometry of the Pd atom is square planar with a slight tetrahedral distortion. The Pd-Cl, Pd-Cla, Pd-N2 and Pd-C1 distances are 2.3010(3) Å, 2.3010(3) Å, 2.1044(14) Å and 1.9739(15) Å respectively. Also angles of Cla-Pd-N2, N2-Pd-Cl, Cl-Pd-C1 and C1-Pd-Cla are 90.37°, 90.37°, 89.63° and 89.63° respectively as shown in Figure 4.2.

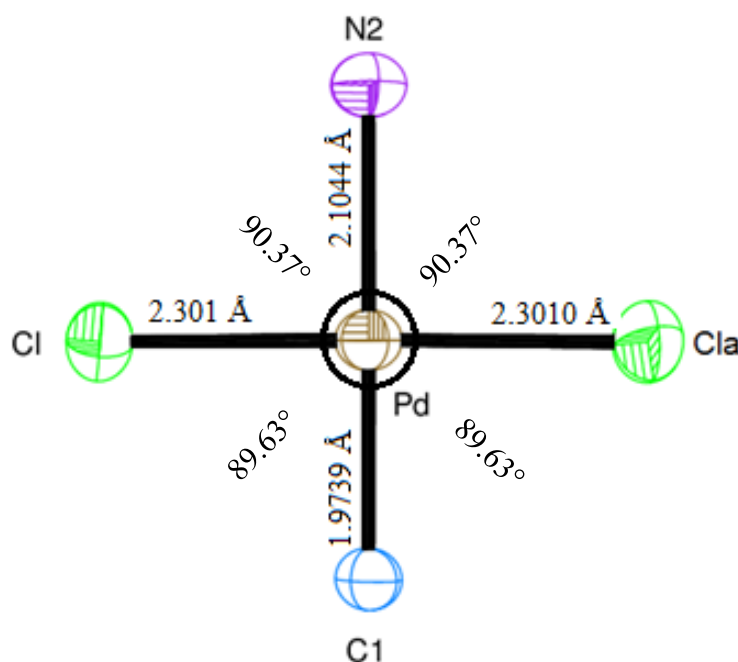


Figure 4.2. Geometric Coordinate of the palladium atom

Table 4.2. Atomic bond lengths (Å) of compound (I)

Bonds	Bond lengths	Symmetry
Pd - C1	1.9739(15)	
Pd - N2	2.1044(14)	
Pd - C11	2.3010(3)	8665
Pd - C11a	2.3010(3)	
C1 - N1	1.3510(14)	
C1 - N1a	1.3510(14)	8665
N2 - C14	1.3243(19)	8665
N2 - C14	1.3243(19)	
C14 - C15	1.384(2)	
C16 - C15	1.357(3)	8665
C16 - C15	1.357(3)	
C8 - O	1.354(2)	
C8 - C7	1.398(2)	
C8 - C3	1.405(2)	
C3 - C4	1.379(2)	
C3 - C2	1.512(2)	
C12 - C13	1.378(2)	
C12 - C11	1.401(2)	
C7 - C6	1.374(3)	
C4 - C5	1.389(3)	
C6 - C5	1.378(3)	
N1 - C11	1.3886(17)	
N1 - C2	1.4581(18)	
C13 - C13	1.390(4)	8665
O - C9	1.4237(19)	
C9 - C10	1.486(4)	
C11 - C11	1.381(3)	8665

Symmetry code [8665]: $I-y, I-x, I/2-z$

Table 4.3. Atomic bond lengths (Å) of compound (I)

Bonds	Bond Angles	Symmetry
C1 - Pd - N2	180.000(7)	
C1 - Pd - C11	89.634(10)	8665
N2 - Pd - C11	90.366(10)	8665
C1 - Pd - C11	89.634(10)	
N2 - Pd - C11	90.366(10)	
C11 - Pd - C11	179.27(2)	8665
N1 - C1 - N1	107.24(14)	8665
N1 - C1 - Pd	126.38(7)	
N1 - C1 - Pd	126.38(7)	8665
C14 - N2 - C14	117.50(18)	8665
C14 - N2 - Pd	121.25(9)	8665
C14 - N2 - Pd	121.25(9)	
N2 - C14 - C15	122.68(18)	
C15 - C16 - C15	118.5(2)	8665
C16 - C15 - C14	119.30(19)	
O - C8 - C7	124.80(15)	
O - C8 - C3	115.93(14)	
C7 - C8 - C3	119.27(17)	
C4 - C3 - C8	119.51(15)	
C4 - C3 - C2	121.04(14)	
C8 - C3 - C2	119.36(14)	
C13 - C12 - C11	116.23(16)	
C6 - C7 - C8	119.82(17)	
C3 - C4 - C5	120.93(18)	
C7 - C6 - C5	121.27(17)	
C6 - C5 - C4	119.14(19)	
C1 - N1 - C11	109.75(10)	
C1 - N1 - C2	125.49(11)	
C11 - N1 - C2	124.69(11)	
C12 - C13 - C13	122.07(10)	8665
N1 - C2 - C3	113.81(11)	
C8 - O - C9	119.78(15)	
O C9 C10	107.01(18)	
C11 - C11 - N1	106.63(7)	8665
C11 - C11 - C12	121.70(10)	8665
N1 - C11 - C12	131.68(14)	
Symmetry code [8665]: <i>I</i> - <i>y</i> , <i>I</i> - <i>x</i> , <i>I</i> / <i>2</i> - <i>z</i>		

In ORTEP diagram as in Figure 4.1 we have the below planes (ring) and Analysis of Short Ring-Interactions with Cg-Cg distance between ring described as the weakest and strongest interactions are 5.8619 Å and 3.7640 Å' respectively between Cg3-Cg3 and Cg3-Cg4' respectively. The details of Cg-Cg interactions can be seen in Table 4.4.

Cg1= (N1/C1/N1a/C11a/C11), Cg2= (N2/C14/C15/C16/C15a/C14a)

Cg3= (C3/C4/C5/C6/C7/C8), Cg4= (C11/C12/C13/C13a/C12a/C11a)

Cg5= (N1/C1/N1a/C11a/C12a/C13a/C13/C12/C11)

Table 4.4. Analysis of Short Ring-Interactions

Cg - Cg	ARU Codes	Distance(Å)	Dihedral Angle(deg)
Cg(1) - Cg(3)	1555	4.6962(9)	69.07
Cg(1) - Cg(3)	2555	4.0867(9)	2.59
Cg(1) - Cg(3)	7555	4.0867(9)	2.59
Cg(1) - Cg(3)	8665	4.6962(9)	69.07
Cg(2) - Cg(3)	1655	5.6081(11)	84.96
Cg(2) - Cg(3)	8655	5.6081(11)	84.96
Cg(3) - Cg(1)	4454	4.0866(9)	2.59
Cg(3) - Cg(1)	7545	4.0866(9)	2.59
Cg(3) - Cg(2)	1455	5.6082(11)	84.96
Cg(3) - Cg(2)	8565	5.6082(11)	84.96
Cg(3) - Cg(3)	2555	5.8619(11)	66.49
Cg(3) - Cg(4)	1555	5.4910(10)	68.64
Cg(3) - Cg(4)	4454	3.7640(10)	2.32
Cg(3) - Cg(4)	7545	3.7640(10)	2.32
Cg(3) - Cg(4)	8665	5.4910(10)	68.64
Cg(4) - Cg(3)	2555	3.7640(10)	2.32
Cg(4) - Cg(3)	7555	3.7640(10)	2.32

ARU Codes [1555] = x, y, z [8655] = $1-y, -x, 1/2-z$
 [2555] = $1/2-y, 1/2+x, 1/4+z$ [4454] = $-1/2+y, 1/2-x, -1/4+z$
 [7555] = $1/2-x, 1/2+y, 1/4-z$ [7545] = $1/2-x, -1/2+y, 1/4-z$
 [8665] = $1-y, 1-x, 1/2-z$ [1455] = $-1+x, y, z$
 [1655] = $1+x, y, z$ [8565] = $-y, 1-x, 1/2-z$

Intramolecular and intermolecular interaction was observed in this crystal structure. There are five intramolecular of hydrogen bonds (Table 4.5), N14-H14...Cl (x,y,z), C12-H12 ...O (x,y,z), C4-H4...N1 (x,y,z), C2-H2A...Cl (x,y,z), and C2-H2B...O (x,y,z) with hydrogen bond length 3.251(002) Å, 3.566(002) Å, 3.096(002) Å, 3.493(001) Å and 2.743(002) Å respectively as in Figure 4.3.

However there are two intermolecular C-H...Cl types of hydrogen bonds C6-H6...Cl ($-x+1/2,+y-1/2,-z+1/4$) and C15-H15...Cl ($-x+1/2+1,+y-1/2,-z+1/4$) with hydrogen-bond length 3.750(002) Å and 3.528(002) Å respectively as shown in Table 4.5.

Table 4.5. Hydrogen-bond geometry (Å, °) of compound (I)

D-H...A	D-H	D-A	H...A	D-H...A
C14 - H14 ... Cl ⁱ	1.056(.020)	3.251(002)	2.748(.021)	109.14(1.31)
C12 - H12 ... O ⁱ	0.973(.026)	3.566(.002)	2.651(.027)	156.83(2.09)
C4 - H4 ... N1 ⁱ	0.930(.002)	3.096(.002)	2.935(.001)	91.13(0.12)
C2 - H2A ... Cl ⁱ	0.970(.001)	3.493(.001)	2.756(.000)	133.22(0.09)
C2 - H2B ... O ⁱ	0.970(.002)	2.743(.002)	2.253(.001)	110.18(0.10)
C6 - H6 ... Cl ⁱⁱ	0.930(.002)	3.750(.002)	2.958(.000)	143.94(0.13)
C15 - H15 ... Cl ⁱⁱⁱ	1.175(.036)	3.528(.002)	2.768(.036)	121.58(2.23)

Symmetry codes: (i) x,y,z
(ii) $-x+1/2,+y-1/2,-z+1/4$
(iii) $-x+1/2+1,+y-1/2,-z+1/4$

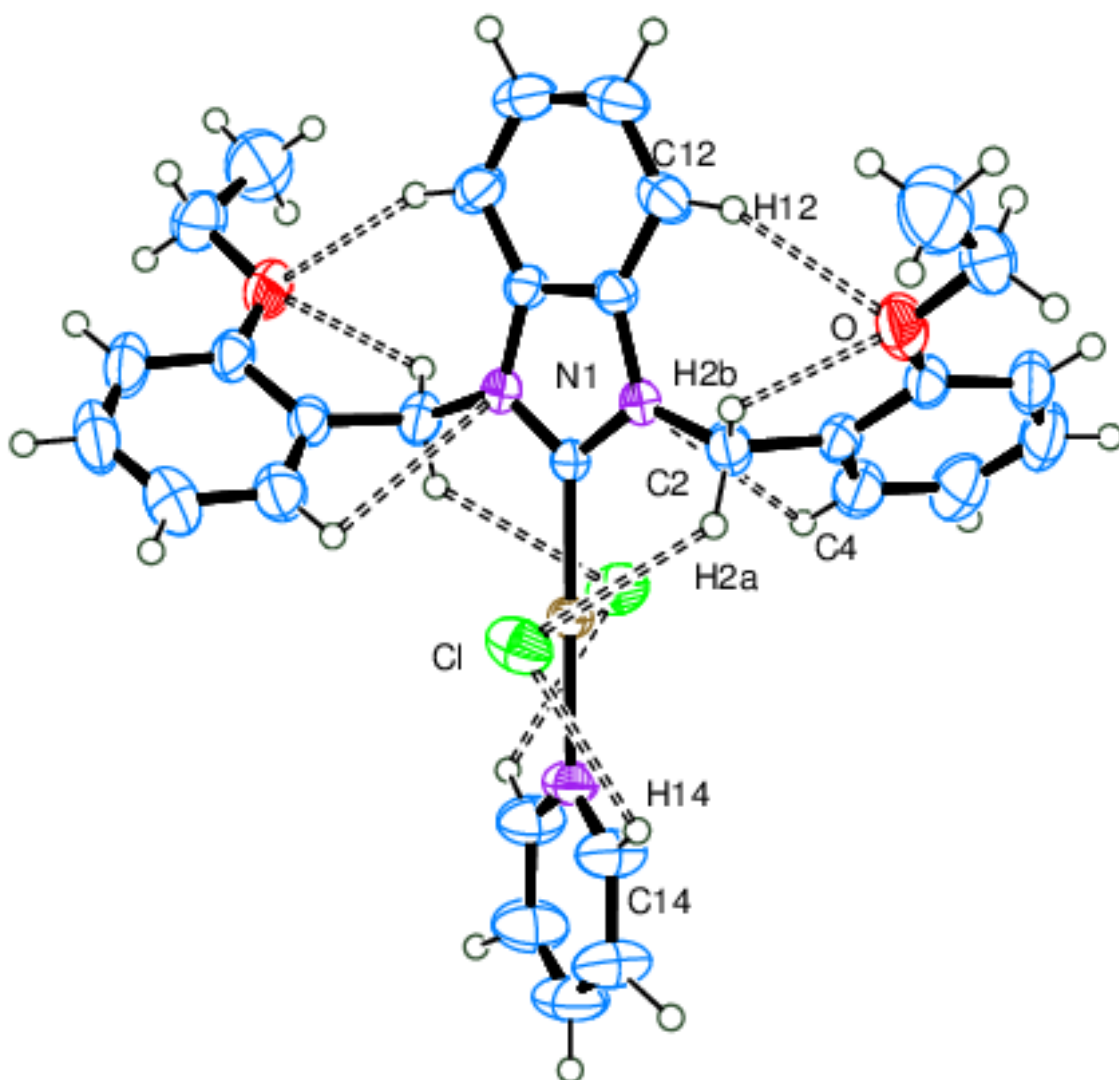


Figure 4.3. Intramolecular hydrogen bonds (dashed lines) of compound (I)

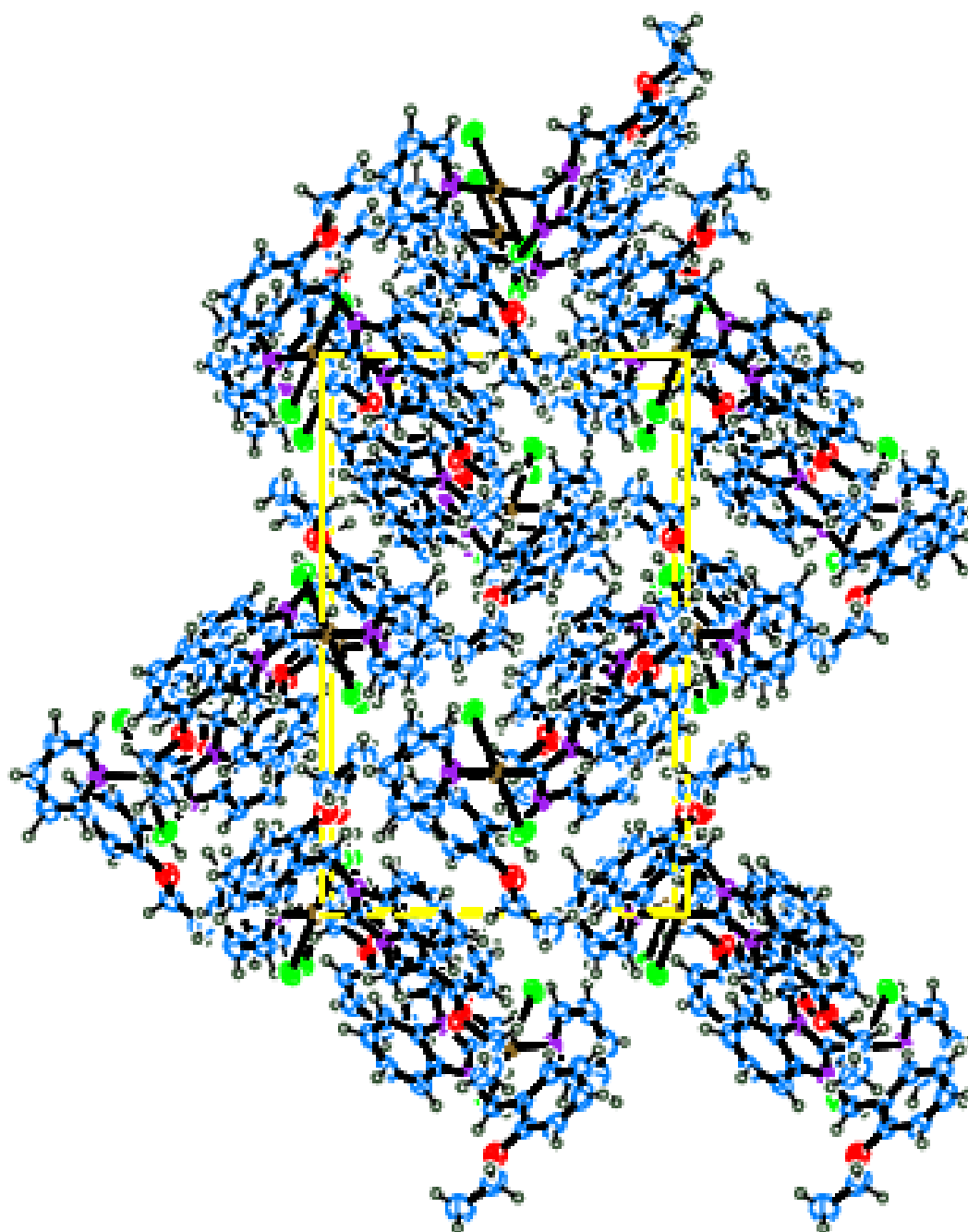


Figure 4.4. Unit Cell packing of compound (I) at (100)

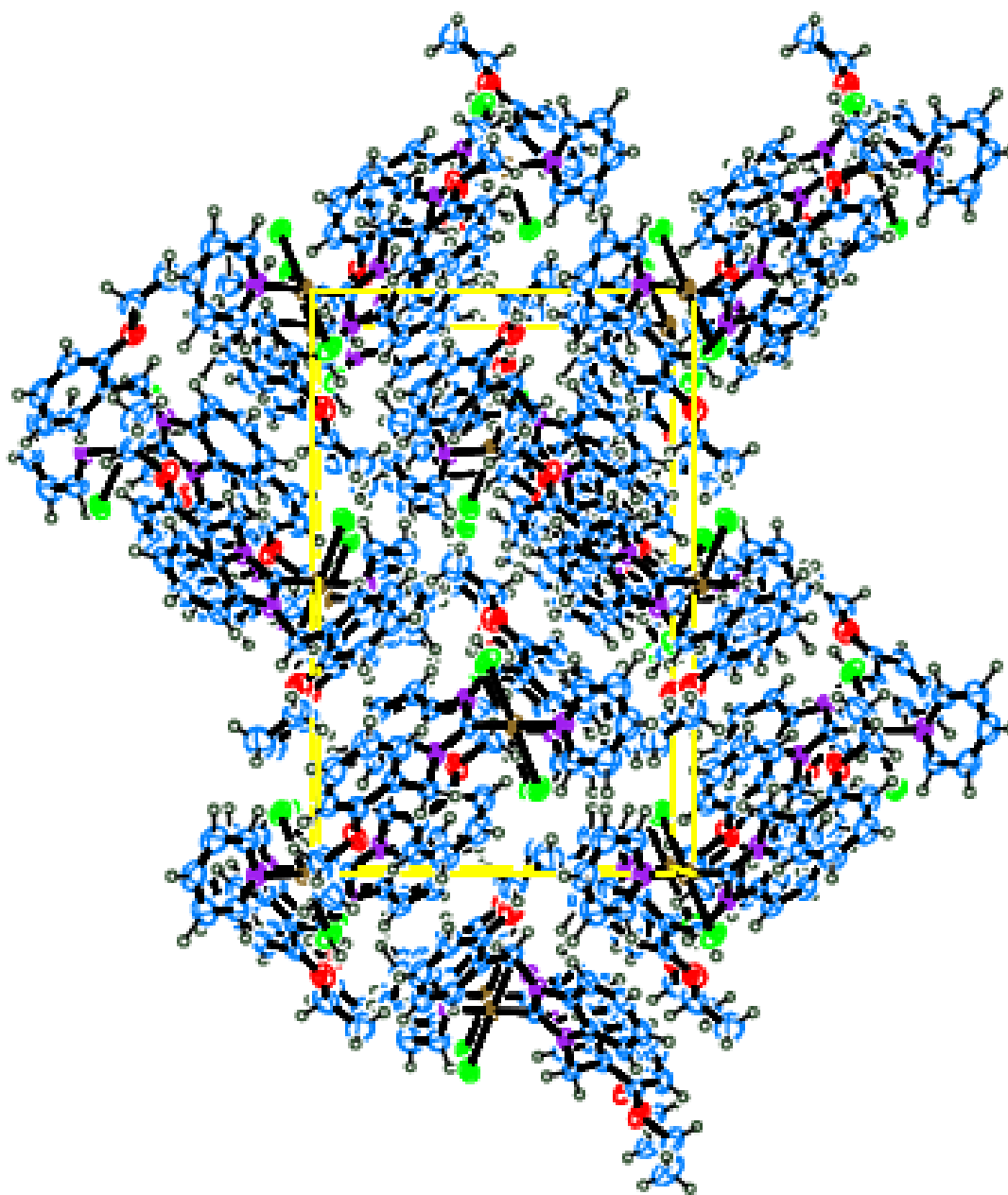


Figure 4.5. Unit Cell packing of compound (I) at (010)

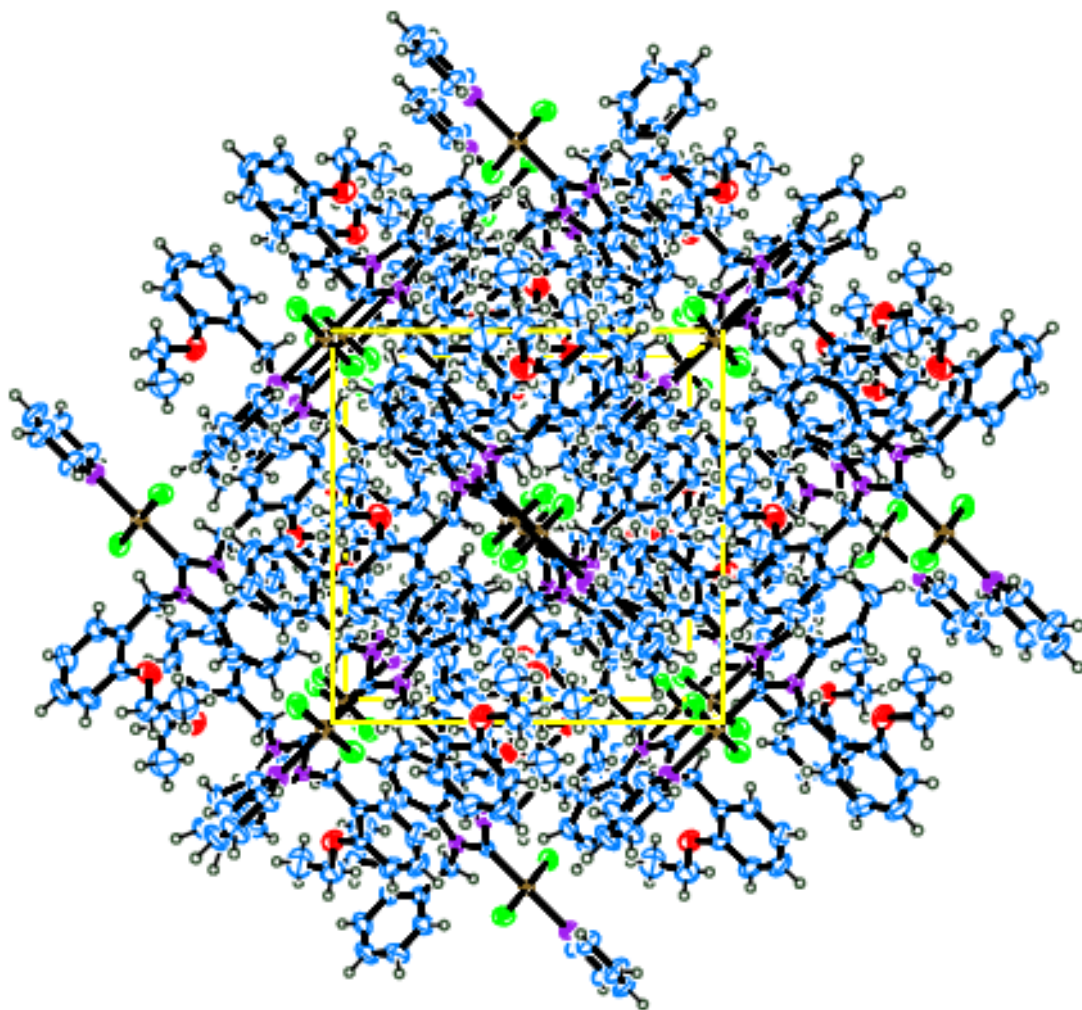


Figure 4.6. Unit Cell packing of compound (I) at (001)

Table 4.6. Fractional atomic coordinates and isotropic or equivalent isotropic displacement parameters (\AA^2) of compound (I)

Atom	X	Y	Z	<i>U</i> _{iso} */ <i>U</i> _{eq}
Pd	0.519519(7)	0.480481(7)	0.2500	0.03240(4)
O	0.12087(9)	0.52374(12)	0.06583(7)	0.0572(3)
N1	0.32405(8)	0.60020(9)	0.20488(6)	0.0327(2)
N2	0.63902(8)	0.36098(8)	0.2500	0.0420(3)
C1	0.40743(8)	0.59257(8)	0.2500	0.0295(3)
C2	0.30454(11)	0.52932(13)	0.14529(8)	0.0397(3)
C3	0.21771(11)	0.44678(12)	0.15824(8)	0.0385(3)
C4	0.22823(15)	0.37090(14)	0.21051(10)	0.0506(4)
C5	0.1526(2)	0.28985(16)	0.21865(11)	0.0636(5)
C6	0.06635(18)	0.28551(16)	0.17336(11)	0.0648(5)
C7	0.05269(14)	0.36107(15)	0.12153(11)	0.0558(4)
C8	0.12764(12)	0.44387(13)	0.11385(8)	0.0428(3)
C9	0.03074(16)	0.52886(18)	0.01995(10)	0.0665(5)
C10	0.0485(3)	0.6216(2)	-0.02775(15)	0.0950(9)
C11	0.26204(10)	0.68930(11)	0.22157(7)	0.0327(2)
C12	0.16796(12)	0.73061(14)	0.19159(9)	0.0435(3)
C13	0.12751(13)	0.82275(13)	0.22167(9)	0.0506(4)
C14	0.66505(16)	0.30897(17)	0.19178(10)	0.0578(4)
C15	0.7434(2)	0.2302(2)	0.18997(12)	0.0720(6)
C16	0.79600(12)	0.20400(12)	0.2500	0.0696(8)
Cl1	0.58447(3)	0.54710(3)	0.14561(2)	0.05250(10)
H2A	0.3708	0.4923	0.1337	0.048
H2B	0.2845	0.5726	0.1050	0.048
H4	0.2868	0.3740	0.2407	0.061
H5	0.1600	0.2392	0.2542	0.076
H6	0.0164	0.2304	0.1780	0.078
H7	-0.0062	0.3571	0.0916	0.067
H9A	0.0246	0.4629	-0.0069	0.080
H9B	-0.0348	0.5388	0.0467	0.080
H10A	-0.0111	0.6280	-0.0594	0.142
H10B	0.0549	0.6862	-0.0005	0.142
H10C	0.1133	0.6105	-0.0541	0.142
H12	0.137(2)	0.687(2)	0.1543(14)	0.076(7)
H13	0.058(2)	0.8482(19)	0.2072(10)	0.066(6)
H14	0.6338(17)	0.3320(17)	0.1425(10)	0.061(5)
H15	0.743(3)	0.176(3)	0.1395(19)	0.114(10)
H16	0.8488	0.1512	0.2500	0.084

Table 4.7. Atomic displacement parameters (\AA^2) of compound compound (I)

Atoms	U_{11}	U_{22}	U_{33}	U_{23}	U_{13}	U_{12}
Pd	0.02816(4)	0.02816(4)	0.04086(7)	0.00298(3)	0.00298(3)	0.00170(5)
O	0.0492(6)	0.0581(6)	0.0644(7)	-0.0036(7)	-0.0205(5)	-0.0077(6)
Cl1	0.04272(17)	0.0586(2)	0.0562(2)	0.02104(17)	0.01158(15)	0.00425(15)
N1	0.0269(4)	0.0298(5)	0.0414(6)	-0.0034(4)	-0.0024(4)	-0.0028(4)
N2	0.0376(5)	0.0376(5)	0.0510(9)	0.0056(6)	0.0056(6)	0.0086(6)
C1	0.0251(4)	0.0251(4)	0.0385(8)	-0.0001(5)	-0.0001(5)	-0.0025(5)
C2	0.0334(6)	0.0454(7)	0.0402(7)	-0.0081(6)	0.0003(5)	-0.0067(6)
C3	0.0342(6)	0.0365(6)	0.0450(7)	-0.0134(6)	0.0021(5)	-0.0035(5)
C4	0.0516(9)	0.0460(8)	0.0542(9)	-0.0058(7)	0.0015(7)	-0.0049(7)
C5	0.0759(13)	0.0464(9)	0.0686(12)	-0.0007(8)	0.0068(10)	-0.0125(9)
C6	0.0623(11)	0.0505(9)	0.0818(13)	-0.0175(9)	0.0131(10)	-0.0250(9)
C7	0.0437(8)	0.0572(10)	0.0665(10)	-0.0227(8)	0.0012(7)	-0.0155(7)
C8	0.0355(6)	0.0439(7)	0.0490(8)	-0.0177(6)	-0.0010(6)	-0.0040(6)
C9	0.0582(10)	0.0702(11)	0.0711(11)	-0.0183(9)	-0.0277(9)	0.0009(10)
C10	0.103(2)	0.0858(17)	0.0959(17)	0.0100(13)	-0.0475(16)	-0.0031(15)
C11	0.0271(5)	0.0307(6)	0.0402(6)	0.0036(5)	0.0021(4)	-0.0010(4)
C12	0.0299(6)	0.0468(8)	0.0540(9)	0.0126(7)	-0.0001(6)	0.0002(6)
C13	0.0371(7)	0.0501(8)	0.0646(9)	0.0191(7)	0.0084(6)	0.0116(6)
C14	0.0594(11)	0.0616(11)	0.0523(9)	-0.0053(8)	0.0021(8)	0.0225(8)
C15	0.0728(14)	0.0679(13)	0.0754(13)	-0.0105(11)	0.0107(10)	0.0306(11)
C16	0.0586(10)	0.0586(10)	0.0918(19)	0.0145(13)	0.0145(13)	0.0291(12)

4.3. Compound II: Dichloro-[1-(2,3,4,5,6-pentamethylbenzil)-3-(2,3,5,6 tetramethyl) benzimidazole-2-ylidene] Ruthenium(II).

Single crystal X-ray diffraction measurements were made on an orange prism shaped crystal of $C_{37}H_{54}Cl_2N_2Ru$ with 0.4x0.25x0.03 mm at 296(2) K on a AXS SMART diffractometer.

Determination of integral intensities, unit cell refinement and data reduction were performed with SAINT-Plus (SAINT-Plus, 2007)

Subsequent data absorption correction was done by SADABS (SADABS, 2007) using multi-scan technique. The space group $P 2_1/n$ with $Z = 4$ for the compound (II), was determined by WinGX. The structure was solved by patterson methods using SHELXTL(Sheldrick, 2008).

Full-matrix least-square refinement on F^2 against all reflections was carried out by SHELXTL (Sheldrick, 2008) All non-hydrogen heavy atoms were refined anisotropically. All H atoms were positioned with idealized geometry and fixed C-H distances for CH, CH₂ and CH₃ at 0.93, 0.97 and 0.96 Å, respectively. Free rotation was permitted for methyl groups. U_{iso} (H) values were set to 1.2 U_{eq} of the carrier atom or 1.5 U_{eq} for methyl groups. A summary of the crystal data can be seen in Table 4.8 and the solid state molecular structure can be seen in Figure 4.7.

Table 4.8. Summary of crystallographic data for compound (II)

Empirical Formula	C₃₂H₄₁Cl₃N₂Ru		
Chemical Formula Weight	661.1		
Crystal System	Monoclinic		
Space Group	P 2 ₁ /n		
Wavelength (Å)	MoKα 0.71073		
a (Å)	8.5084(5)	α (°)	90(0)
b (Å)	25.2249(14)	β (°)	93.677(2)
c (Å)	14.0200 (9)	γ (°)	90(0)
Volume (Å³)	3002.83(5)		
Z	4		
F (000)	1368		
Crystal size	0.4x0.3x0.25		
Absorption correction	Multi-scan		
Theta (θ) range (θ_{min} - θ_{max})	1.6° → 33.2°		
Index ranges	h = -13→13, k = -38→38, l = -21→16		
Reflection collected	45887		
Independent reflections	11203		
Observed reflections (I>2σ(I))	6796		
Refinement method	Full-matrix least-squares on F ²		
Data/restraints/parameter	11203/ 0 /362		
Peak differences in electron density map	Δ _{ρmax} = 2.453 eÅ ⁻³ , Δ _{ρmin} = -1.142 eÅ ⁻³		
Absorption Coefficient (mm⁻¹)	0.813		
R_{int}	0.0697		
R₁, wR₂	0.0728, 0.1977		
R indices (all data)	0.1358		
Goodness of fit S	1.0250		
Temperature (K)	296(2)		

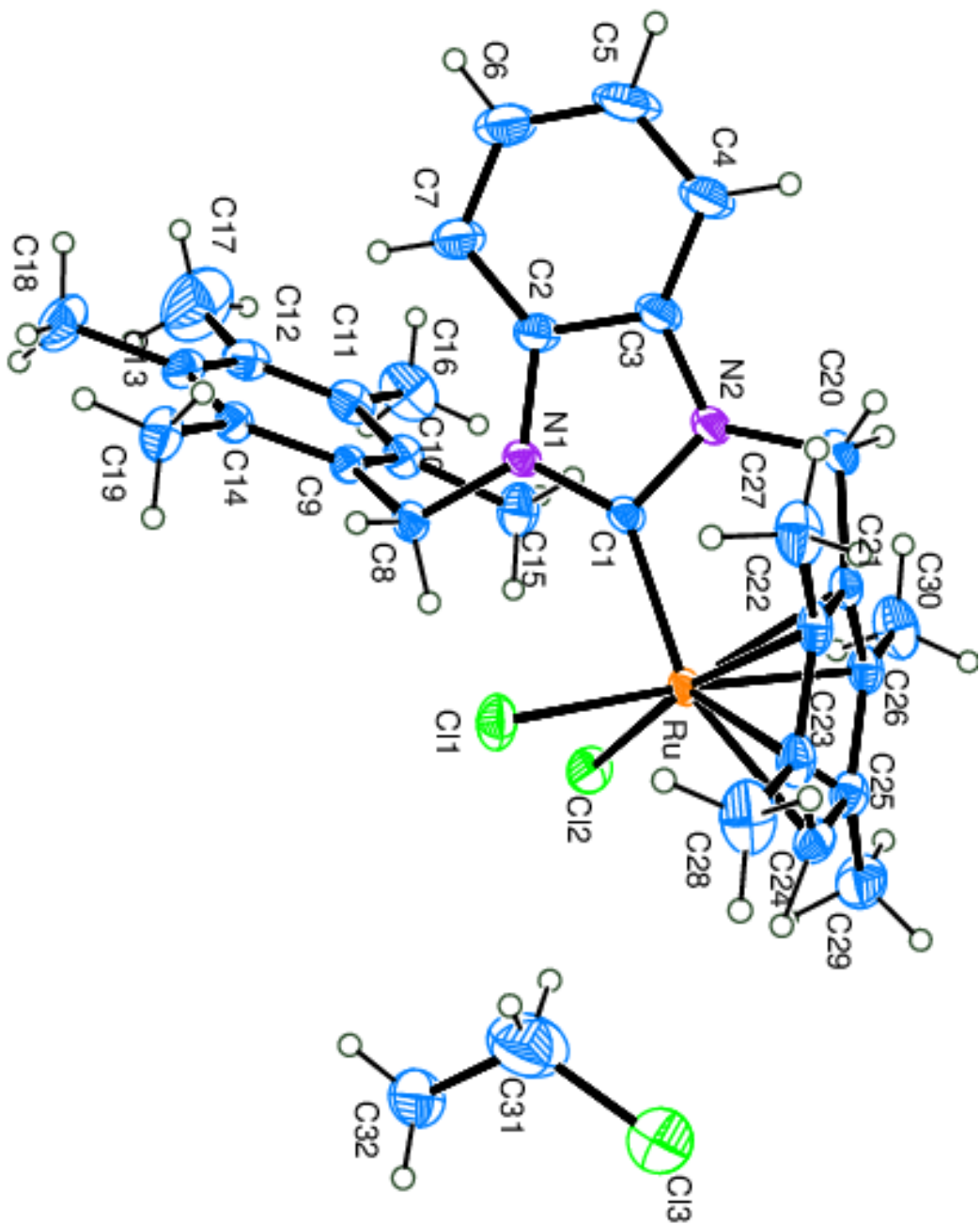


Figure 4.7. Molecular structure of Dichloro-[1,3-bis-(2-etoksibenzil)benzimidazole-2-ylidene] palladium (II) (ORTEP diagram)

The peak differences in electron density map in compound (II) for Ruthenium (II) complex is ($\Delta\rho_{\max} = 2.453 \text{ e}\text{\AA}^{-3}$, $\Delta\rho_{\min} = -1.142 \text{ e}\text{\AA}^{-3}$) has a big difference with comparison to the compound (I) for Palladium complex as ($\Delta\rho_{\max} = 0.366 \text{ e}\text{\AA}^{-3}$, $\Delta\rho_{\min} = -0.226 \text{ e}\text{\AA}^{-3}$).

The peak differences in electron density map for compound (II) were compared with literature, see: Ma et al., (2015); Brietzke et al., (2014); Imhof et al., (2005) we found that our value in this thesis is related to the literature as in Table 4.9. and we mean that our value's in general is normal for Ruthenium (II) complex.

Table 4.9. The comparison of the peak differences in electron density map of previous studies

Related literature	Peak differences in electron density map
Ma et al., (2015), D1	$\Delta\rho_{\max} = 2.661 \text{ e}\text{\AA}^{-3}$, $\Delta\rho_{\min} = -2.296 \text{ e}\text{\AA}^{-3}$
Ma et al., (2015), D2	$\Delta\rho_{\max} = 1.293 \text{ e}\text{\AA}^{-3}$, $\Delta\rho_{\min} = -1.104 \text{ e}\text{\AA}^{-3}$
Brietzke et al., (2014)	$\Delta\rho_{\max} = 1.84 \text{ e}\text{\AA}^{-3}$, $\Delta\rho_{\min} = -1.22 \text{ e}\text{\AA}^{-3}$
Imhof et al., (2005)	$\Delta\rho_{\max} = 2.17 \text{ e}\text{\AA}^{-3}$, $\Delta\rho_{\min} = -1.68 \text{ e}\text{\AA}^{-3}$

The Ruthenium atom Ru(II) centre bonded to seven C atoms and two Cl atoms, the coordination geometry of the Ru atom is a pseudo-tetrahedral environment coordination. The Ru-C1, Ru-C21, Ru-C22, Ru-C23, Ru-C24, Ru-C25, Ru-C26, Ru-Cl1 and Ru-Cl2 bonds distances are 2.0559(48) Å, 2.0918(45) Å, 2.1890(48) Å, 2.2455(54) Å, 2.2726(53) Å, 2.2608(53) Å, 2.1900(51)Å, 2.4141(51) Å and 2.4147(15) Å; respectively, as in Figure 4.8.

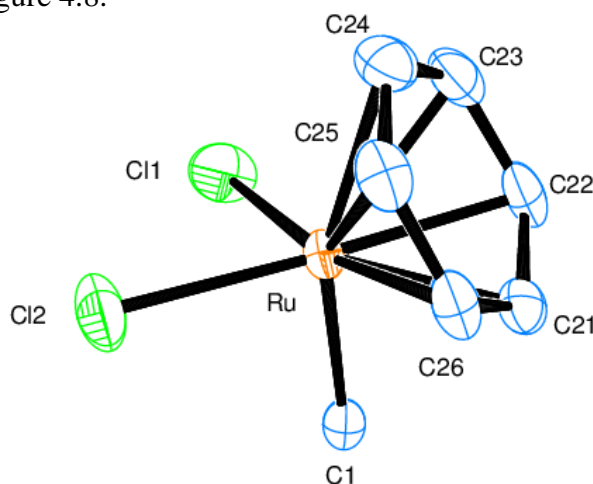


Figure 4.8. Geometric Coordinate of the ruthenium atom

Planes were described as $P_1(C9/C1/C11/C12/C13/C14)$, $P_2(C1/N1/C2/C3/N2)$, $P_3(C2/C3/C4/C5/C6/C7)$, $P_4(Ru/C21/C20/N2/C1)$, $P_5(C21/C22/C23/C24/C25/C26)$. Dihedral angles among these planes P_1-P_2 , P_1-P_3 , P_1-P_4 , P_1-P_5 , P_2-P_3 , P_2-P_4 , P_2-P_5 , P_3-P_4 , P_3-P_5 and P_4-P_5 are 78.21(20), 80.27(20), 71.74(16), 66.87(13), 3.22(25), 8.62(20), 83.84(21), 11.81(22), 82.34(20) and 86.61(15); respectively. In the Table 4.10 can be seen details of dihedral angles among described planes in this crystal.

Table 4.10. Dihedral angles formed by LSQ-planes.

Plane - plane	Angle
$P_1 - P_2$	78.21(20)
$P_1 - P_3$	80.27(20)
$P_1 - P_4$	71.74(16)
$P_1 - P_5$	66.87(13)
$P_2 - P_3$	3.22(25)
$P_2 - P_4$	8.62(20)
$P_2 - P_5$	83.84(21)
$P_3 - P_4$	11.81(22)
$P_3 - P_5$	82.34(20)
$P_4 - P_5$	86.61(15)

However in ORTEP diagram as in Fig. 4.7 we have the following planes (ring) $Cg(1)=(C1/N1/C2/C3/N2)$, $Cg(2)=(C2/C3/C4/C5/C6/C7)$, $Cg(3)=(C9/C10/C11/C12/C13/C14)$, $Cg(4)=(C21/C22/C23/C24/C25/C26)$ and $Cg(5)=(N1/C1/N2/C3/C4/C5/C6/C7/C2)$. Analysis of Short Ring-Interactions with Cg-Cg distance between ring centroids can be seen in Table 4.11.

Table 4.11. Analysis of Short Ring-Interactions

Cg -Cg	ARU Codes	Distance (Å)	Dihedral Angle (deg)
$Cg(3) - Cg(2)$	1555	4.821(4)	80.18
$Cg(3) - Cg(2)$	3566	5.799(4)	80.18
$Cg(3) - Cg(4)$	4454	3.798(3)	0.92
$Cg(4) - Cg(1)$	1555	3.798(3)	83.61
$Cg(4) - Cg(3)$	4555	3.798(3)	0.92

ARU Codes [1555] = x, y, z

[3566] = $-x, 1-y, 1-z$

[4454] = $-1/2+x, 1/2-y, -1/2+z$

[4555] = $1/2+x, 1/2-y, 1/2+z$

Intramolecular and intermolecular interactions was observed in this compound crystal structure. There are nine intramolecular of hydrogen bonds described in Table 4.11, C24-H24...Cl3, C8-H8B...Cl1, C8-H8B...Cl2, C27-H27A...N2, C29-H29B...Cl2, C28-H28B...Cl1, C15-H15B...Cl2, C15-H15C...N1 and C31-H31B...Cl2 with hydrogen-bond length 3.653 Å, 3.312 Å, 3.596 Å, 3.326 Å, 3.355 Å, 3.333 Å, 3.613 Å, 3.058 Å, and 3.742 Å' respectively as in Figure 4.9.

Also there are two intermolecular hydrogen bonds C30-H30A...Cl1 and C20-H20A...Cl2 with hydrogen-bond length 3.727 Å and 3.645 Å respectively as shown in Table 4.11.

Table 4.12. Hydrogen-bond geometry (Å, °) of compound (II)

D-H...A	D-H	D-A	H...A	D-H...A
C24 - H24 ... Cl3 ⁱ	0.980(.005)	3.653(.006)	2.687(.004)	168.73(0.32)
C8 - H8B ... Cl1 ⁱ	0.970(.005)	3.312(.005)	2.943(.002)	103.80(0.31)
C8 - H8B ... Cl2 ⁱ	0.970(.005)	3.596(.005)	2.724(.002)	149.87(0.30)
C27 - H27A ... N2 ⁱ	0.960(.007)	3.326(.008)	2.876(.005)	109.77(0.39)
C29 - H29B ... Cl2 ⁱ	0.960(.008)	3.355(.007)	2.833(.002)	115.16(0.44)
C28 - H28B ... Cl1 ⁱ	0.960(.008)	3.333(.008)	2.718(.001)	122.52(0.46)
C15 - H15B ... Cl2 ⁱ	0.960(.007)	3.613(.007)	2.804(.002)	142.41(0.41)
C15 - H15C ... N1 ⁱ	0.960(.006)	3.058(.008)	2.487(.004)	118.01(0.41)
C31 - H31B ... Cl2 ⁱ	0.970(.014)	3.742(.013)	2.791(.002)	166.78(0.77)
C30 - H30A ... Cl1 ⁱⁱ	0.960(.008)	3.727(.008)	2.878(.001)	147.99(0.43)
C20 - H20A ... Cl2 ⁱⁱⁱ	0.970(.006)	3.645(.006)	2.738(.002)	155.82(0.34)

Symmetry codes: (i) x, y, z

(ii) $x+1/2, -y+1/2+1, +z-1/2$

(iii) $x-1/2, -y+1/2+1, +z-1/2$

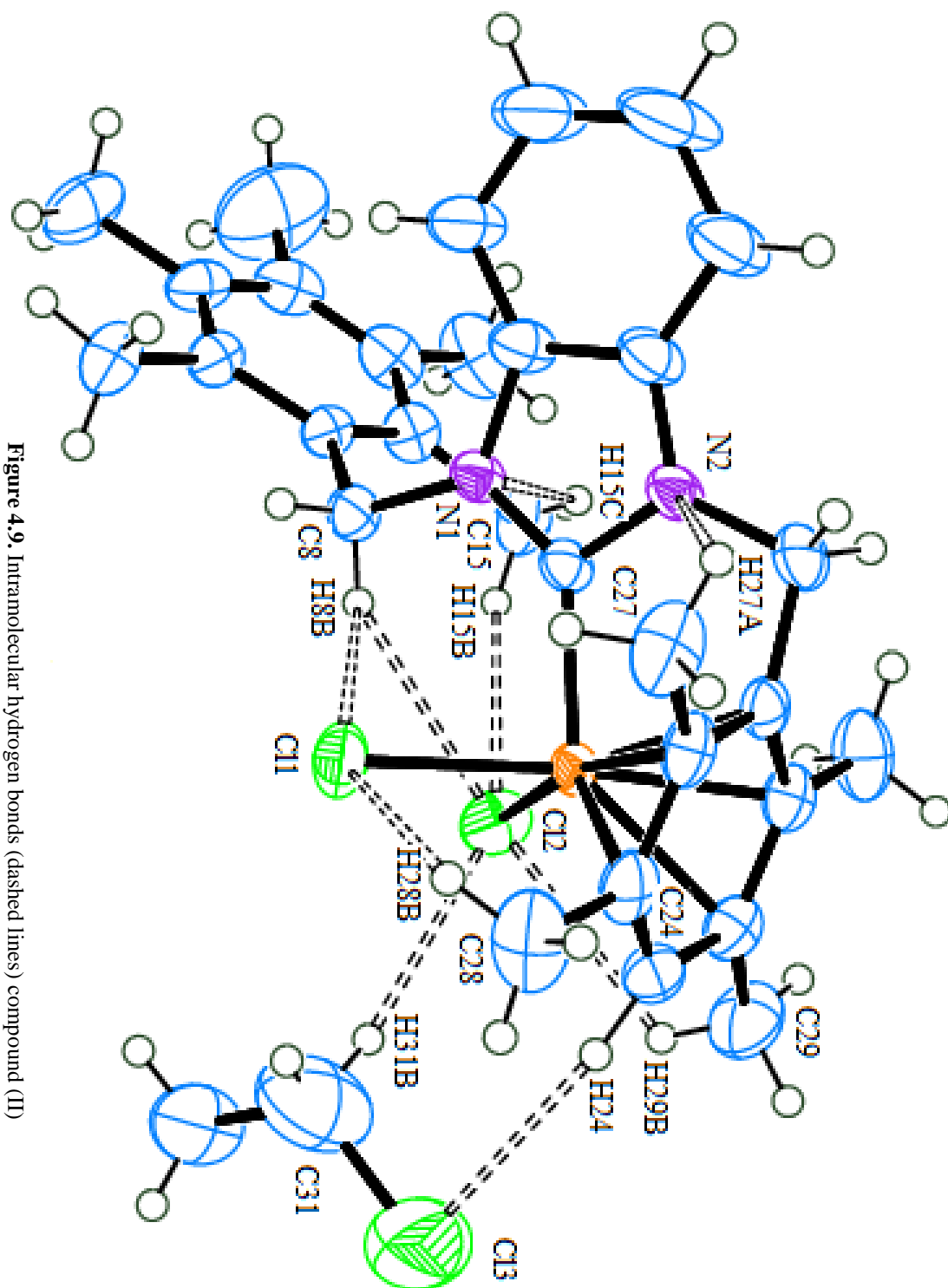


Figure 4.9. Intramolecular hydrogen bonds (dashed lines) compound (II)

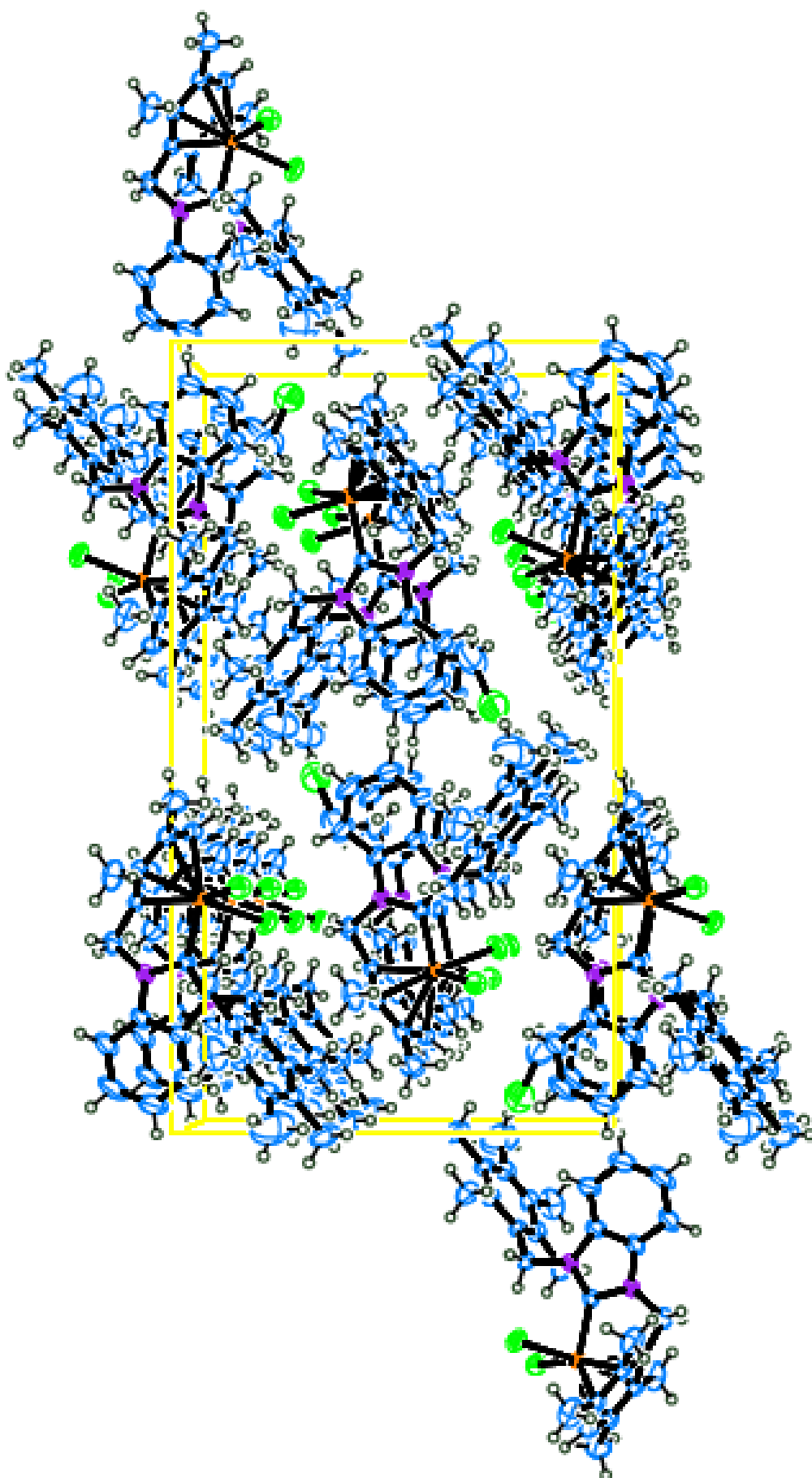


Figure 4.10. Unit Cell packing of compound (II) at (100)

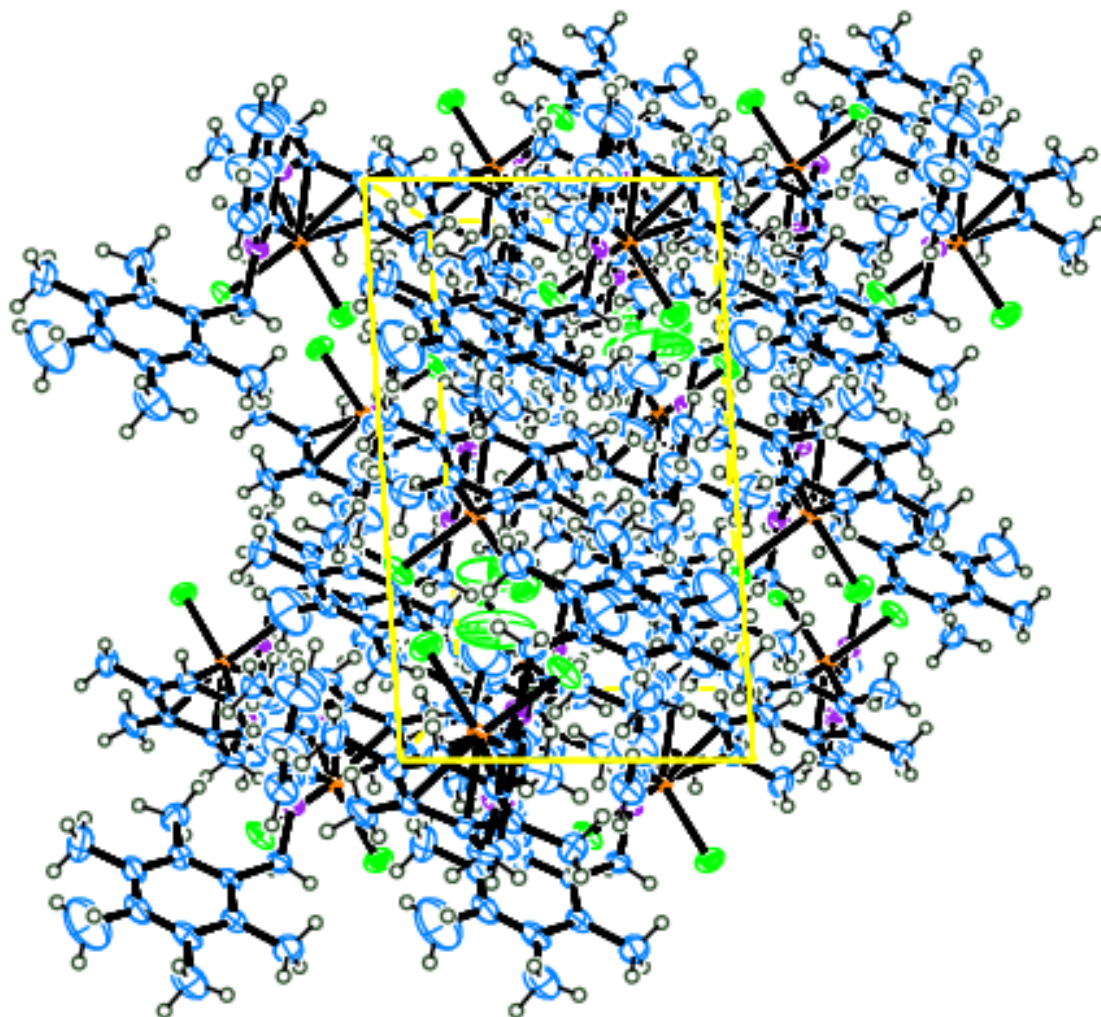


Figure 4.11. Unit Cell packing of compound (II) at (010)

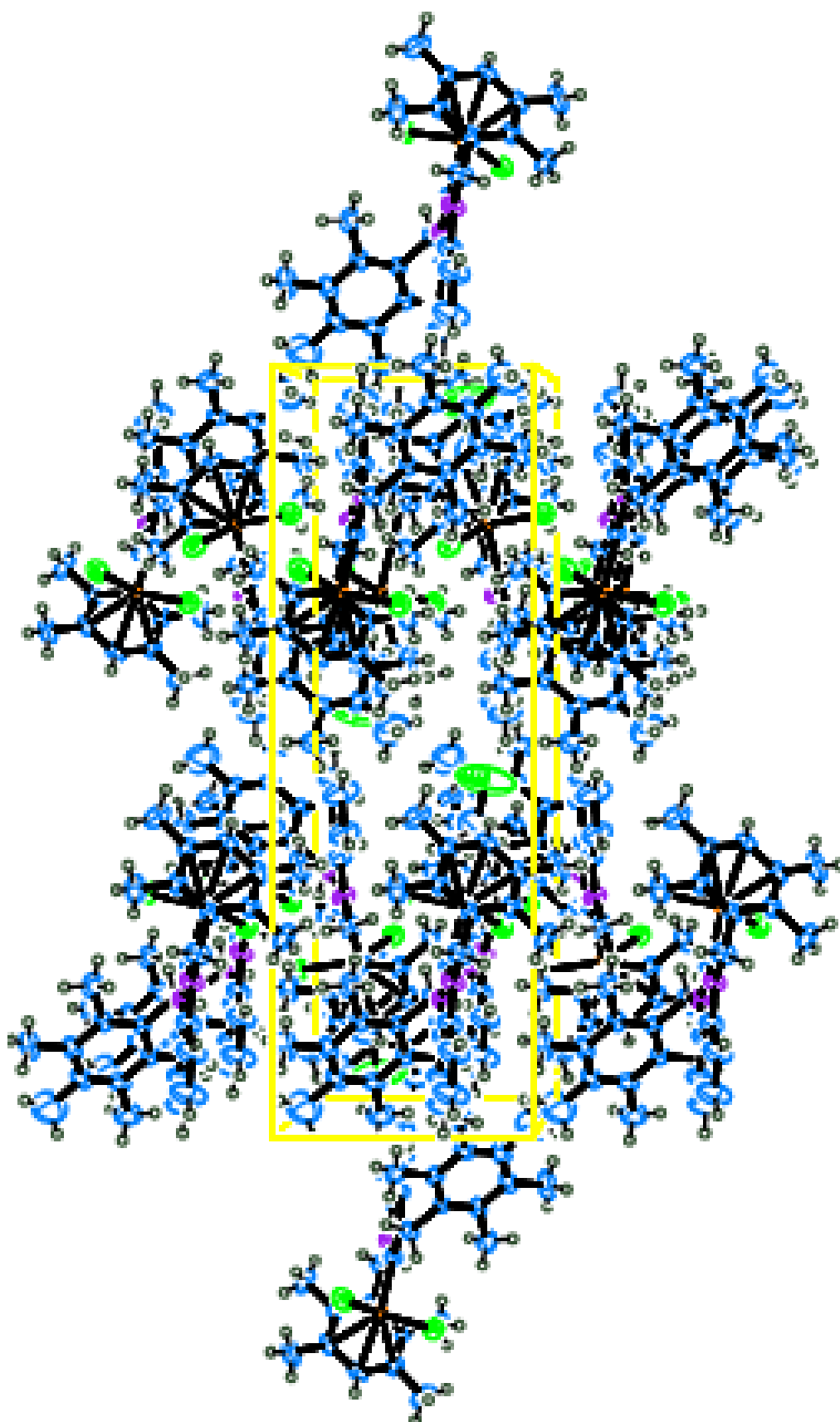


Figure 4.12. Unit Cell packing of compound (II) at (001)

Table 4.13. Fractional atomic coordinates and isotropic or equivalent isotropic displacement parameters (\AA^2) of compound (II)

Atom	Y	y	z	<i>U</i> _{iso} */ <i>U</i> _{eq}
Ru	0.22362(4)	0.20428(1)	0.41413(2)	0.0255(1)
C11	0.35404(18)	0.23391(6)	0.27579(10)	0.0493(5)
C12	-0.01264(18)	0.18991(6)	0.31262(11)	0.0472(4)
N1	0.1334(5)	0.32673(16)	0.3938(3)	0.0300(11)
N2	0.2000(6)	0.29718(17)	0.5362(3)	0.0378(13)
C1	0.1712(6)	0.28200(19)	0.4428(3)	0.0294(11)
C2	0.1484(7)	0.3714(2)	0.4545(4)	0.0391(17)
C3	0.1883(7)	0.3514(2)	0.5456(4)	0.0439(18)
C4	0.2162(10)	0.3843(3)	0.6241(5)	0.064(2)
C5	0.2011(12)	0.4383(3)	0.6077(6)	0.087(3)
C6	0.1635(12)	0.4575(3)	0.5162(6)	0.080(3)
C7	0.1333(8)	0.4252(2)	0.4381(5)	0.052(2)
C8	0.0849(6)	0.3279(2)	0.2904(3)	0.0332(14)
C9	-0.0521(6)	0.36586(19)	0.2670(3)	0.0295(12)
C10	-0.1955(6)	0.3581(2)	0.3068(4)	0.0381(17)
C11	-0.3190(7)	0.3947(3)	0.2895(4)	0.0448(19)
C12	-0.2973(7)	0.4371(2)	0.2299(4)	0.0454(17)
C13	-0.1576(7)	0.4442(2)	0.1853(4)	0.0419(17)
C14	-0.0318(6)	0.4082(2)	0.2036(3)	0.0348(14)
C15	-0.2225(8)	0.3094(3)	0.3680(5)	0.053(2)
C16	-0.4736(8)	0.3880(4)	0.3348(6)	0.072(3)
C17	-0.4276(16)	0.4760(5)	0.2131(12)	0.132(6)
C18	-0.1413(10)	0.4906(3)	0.1176(6)	0.068(3)
C19	0.1214(8)	0.4164(3)	0.1551(5)	0.0510(19)
C20	0.2386(8)	0.2588(2)	0.6122(4)	0.0451(18)
C21	0.2728(6)	0.2071(2)	0.5622(3)	0.0319(11)
C22	0.4216(6)	0.2011(2)	0.5217(3)	0.0357(14)
C23	0.4414(6)	0.1578(2)	0.4583(4)	0.0398(17)
C24	0.3174(7)	0.1209(2)	0.4406(4)	0.0394(17)

C25	0.1727(6)	0.1259(2)	0.4842(4)	0.0367(17)
C26	0.1469(6)	0.1690(2)	0.5461(3)	0.0347(16)
C27	0.5529(7)	0.2400(3)	0.5434(5)	0.0547(19)
C28	0.5879(8)	0.1516(3)	0.4054(5)	0.066(3)
C29	0.0484(10)	0.0856(3)	0.4588(5)	0.063(3)
C30	-0.0071(8)	0.1750(3)	0.5895(5)	0.058(2)
CI3	0.2885(8)	0.04281(14)	0.2207(3)	0.188(3)
C31	0.2440(17)	0.1055(5)	0.1676(9)	0.1209
C32	0.1886(14)	0.1082(4)	0.0690(5)	0.0944
H4	0.24360	0.37084	0.68462	0.0761
H5	0.21636	0.46183	0.65842	0.1041
H6	0.15844	0.49403	0.50731	0.0959
H7	0.10448	0.43873	0.37785	0.0629
H8A	0.17401	0.33855	0.25511	0.0397
H8B	0.05432	0.29246	0.26977	0.0397
H15A	-0.32717	0.31040	0.38965	0.0789
H15B	-0.20975	0.27797	0.33065	0.0789
H15C	-0.14743	0.30918	0.42210	0.0789
H16A	-0.46958	0.35665	0.37383	0.1087
H16B	-0.49262	0.41831	0.37374	0.1087
H16C	-0.55702	0.38461	0.28576	0.1087
H17A	-0.51572	0.46536	0.24806	0.1983
H17B	-0.39246	0.51045	0.23417	0.1983
H17C	-0.45882	0.47722	0.14606	0.1983
H18A	-0.03835	0.49005	0.09328	0.1020
H18B	-0.21965	0.48785	0.06546	0.1020
H18C	-0.15546	0.52322	0.15126	0.1020
H19A	0.11268	0.44737	0.11531	0.0766
H19B	0.20636	0.42100	0.20282	0.0766
H19C	0.14168	0.38599	0.11662	0.0766
H20A	0.32992	0.27033	0.65178	0.0540
H20B	0.15070	0.25452	0.65239	0.0540

4.FINDING AND DISCUSSION

H24	0.32222	0.09690	0.38583	0.0472
H27A	0.51960	0.26620	0.58763	0.0816
H27B	0.64347	0.22165	0.57116	0.0816
H27C	0.57943	0.25712	0.48544	0.0816
H28A	0.57904	0.12044	0.36607	0.0981
H28B	0.60121	0.18214	0.36594	0.0981
H28C	0.67724	0.14814	0.45040	0.0981
H29A	-0.04345	0.09307	0.49280	0.0949
H29B	0.02146	0.08679	0.39126	0.0949
H29C	0.08727	0.05091	0.47596	0.0949
H30A	-0.00493	0.20619	0.62890	0.0869
H30B	-0.08952	0.17833	0.53978	0.0869
H30C	-0.02634	0.14446	0.62783	0.0869
H31A	0.33832	0.12707	0.17533	0.1451
H31B	0.16520	0.12225	0.20462	0.1451
H32A	0.20306	0.14348	0.04550	0.1417
H32B	0.24681	0.08365	0.03261	0.1417
H32C	0.07872	0.09922	0.06287	0.1417

Table 4.14. Atomic displacement parameters (\AA^2) of compound (II)

Atoms	U_{11}	U_{22}	U_{33}	U_{23}	U_{13}	U_{12}
Ru	0.0257(2)	0.0293(2)	0.0208(2)	0.0017(1)	-0.0034(1)	0.0029(2)
Cl1	0.0562(9)	0.0532(8)	0.0401(7)	0.0155(6)	0.0163(6)	0.0128(7)
Cl2	0.0456(8)	0.0443(7)	0.0483(7)	0.0016(6)	-0.0237(6)	-0.0009(6)
N1	0.033(2)	0.030(2)	0.0259(18)	-0.0031(15)	-0.0062(15)	0.0050(16)
N2	0.051(3)	0.036(2)	0.0250(18)	-0.0042(16)	-0.0080(17)	0.009(2)
C1	0.031(2)	0.032(2)	0.0245(19)	-0.0030(16)	-0.0048(18)	0.0027(18)
C2	0.042(3)	0.034(3)	0.040(3)	-0.008(2)	-0.007(2)	0.005(2)
C3	0.055(4)	0.041(3)	0.034(2)	-0.010(2)	-0.010(2)	0.009(3)
C4	0.088(5)	0.055(4)	0.045(3)	-0.020(3)	-0.018(3)	0.015(4)
C5	0.126(8)	0.059(4)	0.070(5)	-0.038(4)	-0.040(5)	0.025(5)
C6	0.120(8)	0.038(4)	0.077(5)	-0.015(3)	-0.025(5)	0.010(4)
C7	0.063(4)	0.036(3)	0.056(4)	-0.010(3)	-0.012(3)	0.007(3)
C8	0.036(3)	0.035(2)	0.028(2)	0.0022(18)	-0.0024(19)	0.007(2)
C9	0.028(2)	0.030(2)	0.029(2)	0.0014(17)	-0.0087(17)	0.0000(18)
C10	0.032(3)	0.044(3)	0.038(3)	0.001(2)	-0.001(2)	0.004(2)
C11	0.034(3)	0.057(4)	0.042(3)	-0.007(3)	-0.008(2)	0.010(3)
C12	0.043(3)	0.045(3)	0.046(3)	-0.008(2)	-0.015(2)	0.013(3)
C13	0.050(3)	0.030(3)	0.043(3)	0.001(2)	-0.019(2)	0.006(2)
C14	0.036(3)	0.035(2)	0.032(2)	0.0030(19)	-0.009(2)	-0.001(2)
C15	0.048(4)	0.061(4)	0.050(3)	0.013(3)	0.013(3)	0.000(3)
C16	0.041(4)	0.104(6)	0.073(5)	-0.009(4)	0.012(3)	0.014(4)
C17	0.125(11)	0.104(9)	0.161(13)	0.027(8)	-0.039(9)	0.018(7)
C18	0.075(5)	0.047(4)	0.079(5)	0.023(3)	-0.021(4)	0.003(3)
C19	0.050(4)	0.052(3)	0.051(3)	0.014(3)	0.003(3)	-0.007(3)
C20	0.062(4)	0.047(3)	0.025(2)	-0.001(2)	-0.008(2)	0.007(3)
C21	0.034(2)	0.037(2)	0.0244(18)	0.0065(18)	-0.0003(17)	0.006(2)
C22	0.028(2)	0.048(3)	0.030(2)	0.014(2)	-0.0078(18)	0.002(2)
C23	0.033(3)	0.049(3)	0.037(3)	0.013(2)	0.000(2)	0.013(2)
C24	0.044(3)	0.035(3)	0.039(3)	0.005(2)	0.002(2)	0.012(2)
C25	0.033(3)	0.039(3)	0.037(3)	0.006(2)	-0.006(2)	-0.004(2)

4.FINDING AND DISCUSSION

C26	0.028(3)	0.044(3)	0.031(2)	0.008(2)	-0.0068(19)	-0.001(2)
C27	0.040(3)	0.071(4)	0.050(3)	0.015(3)	-0.021(3)	-0.020(3)
C28	0.039(3)	0.095(6)	0.064(4)	0.019(4)	0.013(3)	0.024(3)
C29	0.072(5)	0.053(4)	0.063(4)	0.006(3)	-0.005(4)	-0.024(3)
C30	0.039(3)	0.090(5)	0.045(3)	0.011(3)	0.008(3)	0.001(3)
CI3	0.382(8)	0.095(2)	0.085(2)	-0.0012(17)	-0.006(3)	0.059(3)
C31	0.1381	0.1200	0.1000	-0.0352	-0.027(7)	0.024(7)
C32	0.1450	0.0820	0.0503	-0.0015	-0.040(4)	0.049(5)

Table 4.15. Atomic bond lengths (Å) of compound (II)

Bonds	Bond lengths (Å)	Bonds	Bond lengths (Å)
Ru - CL1	2.4141(15)	C27 - H27A	0.9601(69)
Ru - CL2	2.4147(15)	C27 - H27B	0.9600(64)
Ru - C1	2.0559(48)	C27 - H27C	0.9600(68)
Ru - C21	2.0918(45)	C29 - H29A	0.9601(82)
Ru - C22	2.1890(48)	C29 - H29B	0.9599(76)
Ru - C23	2.2455(54)	C29 - H29C	0.9601(72)
Ru - C24	2.2726(53)	C28 - H28A	0.9601(82)
Ru - C25	2.2608(53)	C28 - H28B	0.9597(82)
Ru - C26	2.1900(51)	C28 - H28C	0.9600(68)
C22 - C21	1.4273(71)	C30 - H30A	0.9600(78)
C22 - C23	1.4248(78)	C30 - H30B	0.9600(63)
C22 - C27	1.5040(84)	C30 - H30C	0.9601(78)
C21 - C26	1.4456(71)	C14 - C13	1.4146(77)
C21 - C20	1.5180(76)	C14 - C19	1.5223(86)
C1 - N2	1.3718(60)	C13 - C12	1.3897(88)
C1 - N1	1.3489(61)	C13 - C18	1.5181(94)
C25 - C24	1.4151(79)	C11 - C12	1.3774(86)
C25 - C26	1.4178(74)	C11 - C16	1.5068(96)
C25 - C29	1.4948(92)	C12 - C17	1.4869(146)
C24 - H24	0.9799(54)	C19 - H19A	0.9598(66)
C24 - C23	1.4178(77)	C19 - H19B	0.9600(64)
C26 - C30	1.4871(84)	C19 - H19C	0.9601(66)
C23 - C28	1.4988(90)	C15 - H15A	0.9600(68)
N2 - C3	1.3787(72)	C15 - H15B	0.9600(68)
N2 - C20	1.4621(69)	C15 - H15C	0.9600(65)
N1 - C2	1.4124(66)	C18 - H18A	0.9600(86)
N1 - C8	1.4809(59)	C18 - H18B	0.9599(81)
C2 - C3		C18 - H18C	0.9600(74)
C2 - C7	1.3807(79)	C16 - H16A	0.9600(92)
C9 - C8	1.5283(70)	C16 - H16B	0.9599(92)

4.FINDING AND DISCUSSION

C9 - C10	1.3877(73)	C16 - H16C	0.9601(75)
C9 - C14	1.4078(69)	C17 - H17A	0.9600(150)
C8 - H8A	0.9700(52)	C17 - H17B	0.9601(128)
C8 - H8B	0.9699(50)	C17 - H17C	0.9600(158)
C10 - C11	1.4076(80)	C20 - H20A	0.9701(61)
C10 - C15	1.5240(88)	C20 - H20B	0.9701(64)
C3 - C4	1.3868(88)	C31 - H31A	0.9700(137)
C7 - H7	0.9299(66)	C31 - H31B	0.9699(136)
C7 - C6	1.3764(105)	C31 - C13	1.7783(132)
C4 - H4	0.9300(69)	C31 - C32	1.4335(143)
C4 - C5	1.3843(107)	C32 - H32A	0.9600(92)
C6 - H6	0.9300(73)	C32 - H32B	0.9600(98)
C6 - C5	1.3897(121)	C32 - H32C	0.9601(113)
C5 - H5	0.9300(83)	Number of bond distances: 87	

Table 4.16. Atomic bond angles (deg) of compound (II)

Bonds	Bond angles (deg)	Bonds	Bond angles (deg)
Cl1 - Ru - Cl2	88.92	C2 - C3 - C4	122.02
Cl1 - Ru - C22	101.06	C2 - C7 - H7	121.94
Cl1 - Ru - C21	135.51	C2 - C7 - C6	116.11
Cl1 - Ru - C1	88.76	H7 - C7 - C6	121.95
Cl1 - Ru - C25	136.91	C3 - C4 - H4	121.72
Cl1 - Ru - C24	104.07	C3 - C4 - C5	116.55
Cl1 - Ru - C26	169.08	H4 - C4 - C5	121.74
Cl1 - Ru - C23	88.25	C7 - C6 - H6	118.43
Cl2 - Ru - C22	167.22	C7 - C6 - C5	123.15
Cl2 - Ru - C21	134.11	H6 - C6 - C5	118.43
Cl2 - Ru - C1	94.32	C4 - C5 - C6	120.70
Cl2 - Ru - C25	87.09	C4 - C5 - H5	119.65
Cl2 - Ru - C24		C6 - C5 - H5	119.66
Cl2 - Ru - C26	98.92	C22 - C27 - H27A	109.48
Cl2 - Ru - C23	136.48	C22 - C27 - H27B	109.46
C22 - Ru - C21		C22 - C27 - H27C	109.48
C22 - Ru - C1	93.86	H27A - C27 - H27B	109.48
C22 - Ru - C25	80.17	H27A - C27 - H27C	109.47
C22 - Ru - C24	66.86	H27B - C27 - H27C	109.47
C22 - Ru - C26	70.18	C25 - C29 - H29A	109.48
C22 - Ru - C23	37.46	C25 - C29 - H29B	109.48
C21 - Ru - C1	78.82	C25 - C29 - H29C	109.47
C21 - Ru - C25	68.32	H29A - C29 - H29B	109.47
C21 - Ru - C24	79.85	H29A - C29 - H29C	109.46
C21 - Ru - C26	39.38	H29B - C29 - H29C	109.47
C21 - Ru - C23	68.59	C23 - C28 - H28A	109.46
C1 - Ru - C25	134.32	C23 - C28 - H28B	109.48
C1 - Ru - C24	158.35	C23 - C28 - H28C	109.47
C1 - Ru - C26	98.15	H28A - C28 - H28B	109.47

4.FINDING AND DISCUSSION

C1 - Ru - C23		H28A - C28 - H28C	109.46
C25 - Ru - C24	36.38	H28B - C28 - H28C	109.49
C25 - Ru - C26	37.11	C26 - C30 - H30A	109.47
C25 - Ru - C23	66.54	C26 - C30 - H30B	109.48
C24 - Ru - C26	66.86	C26 - C30 - H30C	109.47
C24 - Ru - C23	36.57	H30A - C30 - H30B	109.47
C26 - Ru - C23	80.84	H30A - C30 - H30C	109.47
Ru - C22 - C21	66.88	H30B - C30 - H30C	109.47
Ru - C22 - C23	73.42	C9 - C14 - C13	118.68
Ru - C22 - C27	130.13	C9 - C14 - C19	121.86
C21 - C22 - C23	118.19	C13 - C14 - C19	119.46
C21 - C22 - C27	121.09	C14 - C13 - C12	119.65
C23 - C22 - C27	120.70	C14 - C13 - C18	120.61
Ru - C21 - C22		C12 - C13 - C18	119.74
Ru - C21 - C26	73.98	C10 - C11 - C12	119.14
Ru - C21 - C20	117.13	C10 - C11 - C16	121.00
C22 - C21 - C26	122.37	C12 - C11 - C16	119.86
C22 - C21 - C20	118.44	C13 - C12 - C11	121.64
C26 - C21 - C20	118.65	C13 - C12 - C17	119.61
Ru - C1 - N2	115.14	C11 - C12 - C17	118.76
Ru - C1 - N1	138.22	C14 - C19 - H19A	109.48
N2 - C1 - N1	105.96	C14 - C19 - H19B	109.47
Ru - C25 - C24	72.26	C14 - C19 - H19C	109.46
Ru - C25 - C26	68.73	H19A - C19 - H19B	109.48
Ru - C25 - C29	130.12	H19A - C19 - H19C	109.48
C24 - C25 - C26	120.49	H19B - C19 - H19C	109.46
C24 - C25 - C29	117.23	C10 - C15 - H15A	109.47
C26 - C25 - C29	122.23	C10 - C15 - H15B	109.47
Ru - C24 - C25	71.36	C10 - C15 - H15C	109.47
Ru - C24 - H24	118.37	H15A - C15 - H15B	109.47
Ru - C24 - C23	70.68	H15A - C15 - H15C	109.48
C25 - C24 - H24	118.37	H15B - C15 - H15C	109.48

C25 - C24 - C23	121.53	C13 - C18 - H18A	109.47
H24 - C24 - C23	118.36	C13 - C18 - H18B	109.48
Ru - C26 - C21	66.64	C13 - C18 - H18C	109.46
Ru - C26 - C25	74.16	H18A - C18 - H18B	109.48
Ru - C26 - C30	128.51	H18A - C18 - H18C	109.47
C21 - C26 - C25	117.51	H18B - C18 - H18C	109.46
C21 - C26 - C30	122.21	C11 - C16 - H16A	109.47
C25 - C26 - C30	120.25	C11 - C16 - H16B	109.48
Ru - C23 - C22	69.12	C11 - C16 - H16C	109.47
Ru - C23 - C24	72.75	H16A - C16 - H16B	109.47
Ru - C23 - C28	128.04	H16A - C16 - H16C	109.47
C22 - C23 - C24	119.78	H16B - C16 - H16C	109.47
C22 - C23 - C28	121.65	C12 - C17 - H17A	109.48
C24 - C23 - C28		C12 - C17 - H17B	109.47
C1 - N2 - C3	110.99	C12 - C17 - H17C	109.48
C1 - N2 - C20	121.97	H17A - C17 - H17B	109.46
C3 - N2 - C20	127.03	H17A - C17 - H17C	109.48
C1 - N1 - C2	110.53	H17B - C17 - H17C	109.46
C1 - N1 - C8	123.84	C21 - C20 - N2	105.80
C2 - N1 - C8	125.62	C21 - C20 - H20A	110.58
N1 - C2 - C3	105.75	C21 - C20 - H20B	110.58
N1 - C2 - C7	132.80	N2 - C20 - H20A	110.58
C3 - C2 - C7	121.44	N2 - C20 - H20B	110.58
C8 - C9 - C10	120.22	H20A - C20 - H20B	108.72
C8 - C9 - C14	119.28	H31A - C31 - H31B	106.96
C10 - C9 - C14	120.49	H31A - C31 - C13	107.43
N1 - C8 - C9	112.59	H31A - C31 - C32	107.43
N1 - C8 - H8A	109.08	H31B - C31 - C13	107.43
N1 - C8 - H8B	109.08	H31B - C31 - C32	107.43
C9 - C8 - H8A	109.07	C13 - C31 - C32	119.57
C9 - C8 - H8B	109.08	C31 - C32 - H32A	109.47
H8A - C8 - H8B	107.83	C31 - C32 - H32B	109.47

4.FINDING AND DISCUSSION

C9 - C10 - C11	120.26	C31 - C32 - H32C	109.47
C9 - C10 - C15	120.51	H32A - C32 - H32B	109.47
C11 - C10 - C15	119.22	H32A - C32 - H32C	109.49
N2 - C3 - C2	106.61	H32B - C32 - H32C	109.46
N2 - C3 - C4	131.28	Number of angles:	195

5. RESULTS AND SUGGESTION

In this study, the experimental geometry of new synthesised two metal complexes single crystals were characterized by using single crystal X-ray diffraction analysis and their molecular and crystal structures were reported. The results for the structures were compared with literature.

Dichloro[1,3-bis-(2-ethoxybenzyl)benzimidazole-2-ylidene] pyridine palladium(II), $C_{30}H_{31}Cl_2N_3O_2Pd$, crystallizes in the tetragonal crystal system space group $P4_12_12$ with $a= 8.5084 \text{ \AA}$, $b= 25.2249 \text{ \AA}$, $c= 14.0200 \text{ \AA}$, $\alpha= 90^\circ$, $\beta= 90^\circ$, $\gamma= 90^\circ$, $V= 2952.77 \text{ \AA}^3$, $Z= 4$, μ (MoK α)= 0.840 mm^{-1} , $R= 0.0393$, $S= 1.028$. The central Palladium Pd atom is bonded to Cl, Cl_a, N, and C atoms it makes a geometry coordinates becomes square planar with a slight tetrahedral distortion.

All the hydrogen atoms in the molecule were identified from the difference electron density map, further idealized and treated as riding with a distance $d(C-H)=0.93 \text{ \AA}$ (for aromatic C-H), $d(C-H)=0.97 \text{ \AA}$ for (CH₂) and $d(C-H)=0.96 \text{ \AA}$ for (CH₃) respectively. In all cases $U_{iso}(H)=-1.2U_{eq}$.

Dichloro-[1-(2,3,4,5,6-pentametilbenzil)-3-(2,3,5,6 tetramethyl) benzimidazole-2-ylidene] Ruthenium(II) crystallizes in the monoclinic crystal system space group $P2_1/n$ with $a= 12.419 \text{ \AA}$, $b= 12.419 \text{ \AA}$, $c= 19.0440 \text{ \AA}$, $\alpha= 90^\circ$, $\beta= 93.677^\circ$, $\gamma= 90^\circ$, $V= 3002.83 \text{ \AA}^3$, $Z= 4$, μ (MoK α)= 0.813 mm^{-1} , $R= 0.0697$, $S= 0.0250$. The Ruthenium atom Ru centre bonded to seven C atoms and two Cl atoms, the coordination geometry of the Ru atom is a pseudo-tetrahedral environment coordination.

All non-hydrogen heavy atoms were refined anisotropically. All H atoms were positioned with idealized geometry and fixed C-H distances for CH, CH₂ and CH₃ at 0.93, 0.97 and 0.96 \AA , respectively. Free rotation was permitted for methyl groups. $U_{iso}(H)$ values were set to $1.2U_{eq}$ of the carrier atom or $1.5U_{eq}$ for methyl groups.

All the bond lengths, bond angles, dihedral angles are within the normal ranges. The crystal structure of compound (I) contains C-H...Cl, C-H...N and C-H...O hydrogen bonds and of compound (II) contains C-H...Cl and C-H...N hydrogen bonds.

5. RESULTS AND SUGGESTION

The molecules of two compounds are linked by intermolecular C-H... π and π - π interactions, forming a three dimensional network.

The implications of the determined crystal structures are discussed in terms of the relevant literature in each case.

Crystal structure analysis is very important because physical and chemical properties of crystalline materials are relevant to crystal and molecular structure.

REFERENCES

- Blow, D., 2002, *Outline of Crystallography for Biologists*, Oxford University Press, New York: p 236.
- BOB B. HE, 2009, *Two Dimensional X-ray Diffraction*, Printed in the United States of America, 1-3
- Bragg, L. W., 1983, The diffraction of short electromagnetic waves by a crystal, *Proc. Camb. Phil. Soc.* 17 part 1, 43-57.
- Brietzke, Falko Otto Rottke, Alexandra Kelling, Uwe Schilde and Hans Jurgen Holdt, 2014, *Acta Cryst.* (2014). E70, 265–268.
- Çetinkaya, Engin C, etinkaya , Maurice Brookhart and Peter S. White , 1998, *Journal of Molecular Catalysis A: Chemical* 142 (1999) 101–112.
- Cheng, Zhao-Ji Li, Yao Kang, Yu-Biao Chen, Ye-Yan Qin, Yi-Hang Wen and Yuan-Gen Yao, *Acta Cryst.* (2002). E58, m768±m769.
- Chiririwa, Reinout Meijboom, Samson O. Owalude, Uche B. Eke and Charmaine Ardernea, *Acta Cryst.* (2011). E67, m1096.
- Clark and Barbara L. Dutrow, 2007, Schematic of 4-circle diffractometer online available at: <http://serc.carleton.edu/details/images/8400.html>. Access Date: 10.12.2014.
- Clegg, W., Blake, J. A., (2009), *Crystal structure analysis: Principles and practice* (2nd edition), Oxford University Press.
- Cullity, 1956, *Elements of X-ray diffraction*, Printed in the United States of America, Addison-wesley publishing company, 42-44
- Cullity, B.D., 1978, *Elements of X-ray Diffraction*, 2nd ed. Reading, Massachusetts, Addison Wesley publishing company inc.

REFERENCES

- Donald E. Sands, 1975, *Introduction to Crystallography*, University of Kentucky, Dover Publications, Inc, New York, This Dover edition first published in 1993, 92
- Elder, R. F., Gurewitsch, M. A., Langmuir, V. R., Pollock, H. C., 1947, Radiation from electrons in a synchrotron, *Physical review*, 71, 829-830
- Eric Lifshin (Ed.), 1999, *X-ray Characterization of Materials*, WILEY-VCH Verlag GmbH, Germany, 5-8
- Friedrich, P. Knipping and M. Laue, 1952, "Interferenz - Erscheinungen bei Röntgenstrahlen". *Die Naturwissenschaften*, 16, 361, 1952. doi:10.1007/BF00646957.
- Glusker, J. P.; Lewis, M.; Rossi, M., 1994, *Crystal Structure Analysis for Chemists and Biologists*, WILEY-VCH Verlag GmbH, Germany, pp. 854.
- Hahn, T. (Ed.), 1983, *International tables for crystallography (volume A)*, Published for the International Union of Crystallography by Reidel.
- Helliwell, R. J., (1992), *Macromolecular crystallography with synchrotron radiation*, Cambridge University Press
- Helmer Fjellvåg, 1994, KJ/MV 210, University of Oslo.
- Hsueh, Sheng-Yuan Su and Chu-Chieh Lin, 2006, *Acta Cryst.* (2006). E62, m1784–m1786.
- Huxham, Elizabeth L.S. Cheu, Brian O. Patrick and Brian R. James *Inorganica Chimica*, 2003, *Acta* 352 (2003) 238_/246.
- Imhof, Kathi Halbauer and Helmar Görls, 2005, *Acta Cryst.* (2005). E61, m2130–m2132, doi:10.1107/S1600536805030461.
- Jindabot, Kriengkamol Teerachanan, Pech Thongkam, Supavadee Kiatisevi, Tossapol Khamnaen , Phairat Phiriyawirut, Sumate Charoenchaidet, Thanasat

- Sooksimuang, Palangpon Kongsaree and Preeyanuch Sangtrirutnugul, 2014, *Journal of Organometallic Chemistry* 750 (2014) 35e40.
- Klug, H.P. Alexander, L.E.S, 1974, *X-ray Diffraction Procedures. For Polycrystalline and Amorphous Materials*, 2nd ed., New York, John Willey and Sons
- L. Smart, E. Moore, 2001, *Solid State Chemistry*, Second ed..
- L.J. Poppe, V.F. Paskevich, J.C. Hathaway, D.S. Blackwood, 2001, X-ray tube image, Online Available at: <http://pubs.usgs.gov/of/2001/of01-041/htmldocs/images/xrdtube.jpg>. Access Date: 20.3.2015
- Lee, M. R., *Meteoritics*, (1994) 29, 898.
- Lipson, H., and W. Cochran, 1966, *The Determination of Crystal structure*, Cornell University Press, Ithaca, New York , pp. 9-6, 66-69
- Lu, Hui-Jun Xu and Xue-Tai Chen, 2009, *Inorganic Chemistry Communications* 12 (2009) 887–889
- Martin T. Dove, 2003, *Structure and Dynamics: An Atomic View of Materials*, Oxford University Press, New York. 199.
- Max Perutz, julio de, 1996, Churchill College, Cambridge, 21 screw axis image, Online Available at: http://www.xtal.iqfr.csic.es/Cristalografia/archivos_07/helicoidal.jpg. Access Date :10.3.2015
- Mellor, J. W., 1955, *Higher Mathematics for students of Chemistry and Physics*, Dover, New York.
- Molloy, C. K., 2004, *Group theory for chemists: fundamental theory and applications*, Horwood.
- Muchmore, S. W., 1999, *Acta Crystallogr., Sect. D: Biol. Crystallogr.*, D55, 1669.

REFERENCES

- Müller, P., Herbst-Irmer, R., Spek, A.L., T.R. Schneider, M. Sawaya, 2005, *Crystal Structure Refinement*, Oxford University Press.
- O'Brien, E.A.B. Kantchev, C. Valente, N. Hadei, G.A. Chass, A. Lough, A.C. Hopkinson and M.G. Organ, 2006, *Chem. Eur. J.* 12 (2006) 4743.
- Ojwach, Ilia A. Guzeiand J. Darkwa, 2008, *Journal of Organometallic Chemistry* 694 (2009) 1393–1399.
- Patterson, L. A., 1935, A direct method for the determination of the component of interatomic distances in crystals, *Z. Krist.* 90, 517-542
- Putnis, A., 1992, *Introduction to Mineral Sciences*, Cambridge, UK: Cambridge University Press, pp. 41-80.
- S. P. Timoshenko and J. N. Goodier, 1970, *Theory of Elasticity*, McGraw-Hill, New York.
- SADABS, 2007, Bruker AXS User Manual, Inc., In Madison, WI.
- SAINT-Plus, 2007, Bruker AXS User Manual, Inc., In Madison, WI.
- Sanat K. Chatterjee, 2008, *Crystallography and the World of Symmetry*, Springer Series in materials science 113, India, 44-45.
- Shafranovskii I I and Belov N V, 1962, *50 Years of X-ray Diffraction*, ed. Paul Ewald (Springer): 351.
- Sheldrick, G. M., 2008, *Acta Crystallogr., Sect. A: Found. Crystallography*, pp.64, 112.
- Sheldrick, H. G., Schneider, R. T., (1997), *SHELXL: High resolution refinement*, *Methods in enzymology*, P: 277, 319-343.
- Svetlana V. Kravtsova, Ilya P. Romm, Adam I. Stash and Vitaly K. Belsky, 1996, *acta crystallographica section c* issn 0108-2701.

Ted Janssen, Gervais Chapuis and Marc de Boissieu, 2007, *Aperiodic Crystals From Modulated Phases to Quasicrystals*, Oxford University Press, 147-148.

User manual, 2001, Smart Apex, version 5, M86-E04015 -1001, 2001, pp. 3-6.

User Manual, 2006, Bruker AXS, APEX2 version 2, Part Number: M86-E01078, pp.3-5.

W. Clegg, 2005, in Chapter 2: Space Group Determination - X-ray Structure Analysis 10th BCA/CCG Intensive School.

W. Clegg, A. J. Blake, R. O. Gould, P. Main, 2001, *Crystal Structure Analysis Principles and Practice*, OUP.

Woolfson, M. M., 1997, *An introduction to X-ray crystallography* (2nd edition), Cambridge University Press.

Zakhia Moore, 2008, *Application of X-ray Diffraction Methods and Molecular Mechanics Simulations to Structure Determination and Cotton Fiber Analysis*, Theses and Dissertations, Doctor of Philosophy In the Department of Chemistry, University of New Orleans.

CURRICULUM VITAE

Full Name: Sirwan Salih Hasan

Nationality: Iraqi, Kurdi

Date of Birth: 10/10/1986

Martial Status: Single

Address: Iraq, Duhok

E-mail: sirwan.hasan@hotmail.com

Education

- 2001-2004: High School in Duhok, Iraq
- 2004-2009: Bsc in Physics at University of Duhok, College of Education, Physics Deptment, Duhok, Iraq

Language Coalification

- Kurdish: Mother tongue
- English: Excellent in both (Written & Spoken)
- Arabic: Excellent in both (Written & Spoken)
- Turkish: Good in both (Written & Spoken)

Work History

- Physics teacher at high school since 2010, Duhok
- Member of the Kurdistan Teachers Union since 2010 .
- Member of Lalish Cultural and Social center since 2004, Duhok